

Helicity amplitudes in massless QED to higher orders in the dimensional regulator

Thomas Dave^{1,*} and William J. Torres Bobadilla^{1,†}

¹*Department of Mathematical Sciences, University of Liverpool, Liverpool L69 3BX, U.K.*

We analytically calculate one- and two-loop helicity amplitudes in massless QED, by adopting a four-dimensional tensor decomposition. We draw our attention to four-fermion and Compton scattering processes to higher orders in the dimensional regulator, as required for theoretical predictions at N³LO. We organise loop amplitudes by proposing an efficient algorithm at integrand level to group Feynman graphs into integral families. We study the singular structure of these amplitudes and discuss the correspondence between QED and QCD processes. We present our results in terms of generalised polylogarithms up to transcendental weight six.

I. INTRODUCTION

Precision physics plays an increasingly important role in research at particle colliders. In recent years, there have been many developments in multi-loop calculation techniques needed to compute scattering amplitudes at increasing perturbative orders in Quantum Field Theories, where their expansion parameter exactly corresponds to the strong coupling constant α_S in Quantum Chromodynamics (QCD) and the fine structure constant α in Quantum Electrodynamics (QED) [1, 2].

Many efforts have been put in efficiently calculating scattering amplitudes of QCD processes to the highest possible perturbative order [3]. In the current frontier, theoretical predictions for collider experiments at high energies are aiming at reaching the best accuracy. After the successful automation of tree-level and one-loop scattering amplitude computations, which led to the next-to-leading order (NLO) revolution, the attention has now shifted towards developing innovative strategies for calculating multi-loop scattering amplitudes to enable theoretical predictions beyond NLO (NNLO and beyond).

Focusing on QCD theoretical predictions for four-parton scattering at NNLO [4–7] and N³LO [8–11], we observe a clear approach, especially at N³LO, for the analytic evaluation of scattering amplitudes required at this perturbative order. By employing the method of differential equations [12–14] alongside integral-level relations satisfied by Feynman integrals [15, 16], these results have become accessible.

Interestingly, less attention has been devoted to the calculation of similar processes that appear in QED. The construction of those massless scattering amplitudes up to two loops was indeed performed a long time ago [7, 17, 18] but to date, there has not been an extension of these results. Moreover, recent attention has been given to constructing these two-loop scattering amplitudes by keeping the dependence on the lepton masses [19–27], motivated by studying physics at low energies [28, 29]. The presence of the lepton masses certainly increases the complexity in the evaluation of the

constituents of the amplitudes, the Feynman integrals, whose efficient numerical evaluation is still an undergoing problem [30].

In this work, we are interested in extending the results of Refs. [7, 17, 18] by analytically calculating massless QED scattering amplitudes needed for N³LO theoretical predictions. Owing to the dimensional regularisation, we begin our work by calculating, from a diagrammatic approach, one- and two-loop scattering amplitudes to higher orders in the dimensional parameter $\epsilon = (4 - D)/2$. Unlike previous calculations in QED, we adopt a tensor decomposition of scattering amplitudes, this immediately allows us to express helicity amplitudes and loop interference terms.

Because in a tensor decomposition of a scattering amplitude the number of tensor structures grows according to the loop order when considering arbitrary space-time dimensions, we profit from the information that external particles live in four space-time dimensions. Specifically, for a given physical process, this allows us to have the number of tensor structures equal to the number of independent helicity states, regardless of the loop order [31–33]. Thus, for the construction of loop amplitudes, we opt to use the 't Hooft-Veltman dimensional regularisation scheme [34] to regulate ultraviolet (UV) and infrared (IR) divergences. This requires us to consider internal loop momenta in D dimensions [35]. We remark that any discrepancy between regularisation schemes is overcome once IR and UV divergences are removed in the construction of a finite remainder, since additional terms that behave as $D - 4$ vanish in the four-dimensional limit.

Due to the number of Feynman diagrams that start appearing at two loops (and the subsequent computation at three loops [36]), we establish a path to organise our calculation, aimed at minimising the required computations. In particular, we provide a method for grouping Feynman diagrams into integral families through matrix transformations, with the motivation of performing operations at integrand level instead of integral level. Once we have our independent integrand families, we proceed by calculating integration-by-parts identities to express our form factors in terms of master integrals that admit a d log representation [37, 38]. The organisation of our form factors in terms of these master integrals facilitates the computation of the complete scattering amplitude.

* tcldave@liverpool.ac.uk

† torres@liverpool.ac.uk

In the sense that possible crossings of kinematics are carried out at this point. We emphasise this simplification in calculations that involve four leptons. With these sets of integrals at hand, we calculate the analytic expressions of master integrals in terms of generalised polylogarithms up to transcendental weight six [39]. Thus, allowing us to construct the form factors that describe the QED processes:

$$e^+e^- \rightarrow \mu^+\mu^-, \quad (1a)$$

$$e^+\mu^- \rightarrow e^+\mu^-, \quad (1b)$$

$$e^+e^- \rightarrow e^+e^-, \quad (1c)$$

$$e^+e^- \rightarrow \gamma\gamma. \quad (1d)$$

Lastly, once UV renormalisation and IR subtraction are employed to construct finite remainders for the form factors of the processes (1), we construct their non-vanishing helicity amplitudes. Due to the similarities between QED and QCD, we make use of known results in QCD to validate our results. This is carried out by finding linear combinations of Abelian diagrams in QCD.

The remainder of the paper is organised as follows. In Sec. II, we discuss the setup of our calculations and the techniques that we utilise to obtain our analytical results. We outline in Sec. III the procedure to construct the finite remainder of the form factors by performing UV renormalisation and IR subtraction. Then, we discuss our results in Sec. IV and perform crosschecks against QCD results in Sec. V. Lastly, we draw our conclusions and discuss future directions in Sec. VI. Additionally, we include four appendices to provide supplementary details. In Appendix A, we present the grouping of two-loop diagrams involved in processes (1a) and (1d); Appendix B lists the integral families required for these processes; Appendix C contains the infrared subtraction constants. In the arXiv submission of this paper, we include ancillary files containing results for the QED processes discussed in the following sections, with further information on these files provided in Appendix D.

II. FORMALISM AND TECHNIQUES

In this section, we provide an overview of the techniques that we use to perform our calculations. We begin by discussing the kinematic setup that we use throughout this paper as well as the perturbative approach to scattering amplitude calculations. We then discuss the tensor decomposition approach to the calculation of scattering amplitudes that we adopt in this paper. We then introduce a novel method that allows us to group sub-topologies to parent topologies via shifts in the loop momenta at integrand level using linear algebra. Lastly, we briefly summarise our adopted strategy to reduce two-loop scattering amplitudes to canonical bases of master integrals. With this formalism at hand, we apply these techniques to the processes relevant for our calculation in Sec. IV.

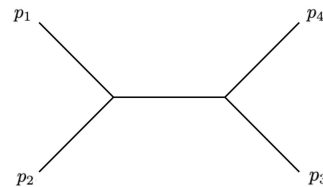


FIG. 1: Representative $2 \rightarrow 2$ process with the adopted ordering of external momenta.

A. Kinematics and Setup

Each of the processes we are considering consists of four particles, we label their corresponding momenta by p_1, p_2, p_3 and p_4 . The ordering of these momenta can be seen in Fig. 1. We consider all external particles to be outgoing so that $p_1 = -p_2 - p_3 - p_4$ is true by momentum conservation. As we are working in massless QED, we have $p_i^2 = 0$ for $i = 1, 2, 3, 4$.

We also define the Mandelstam variables as:

$$s = (p_3 + p_4)^2 = 2p_3 \cdot p_4, \quad (2a)$$

$$t = (p_2 + p_3)^2 = 2p_2 \cdot p_3, \quad (2b)$$

$$u = (p_2 + p_4)^2 = 2p_2 \cdot p_4. \quad (2c)$$

Similarly, by momentum conservation, we can eliminate one of these variables via $u = -s - t$. Utilising this relation, we are able to express our amplitudes in terms of s and t .

We evaluate the processes (1) in the production region,

$$s > 0, \quad t, u < 0. \quad (3)$$

Because of momentum conservation, we introduce a dimensionless variable,

$$x = -\frac{t}{s}. \quad (4)$$

so that the scattering amplitudes are evaluated in the region $x \in (0, 1)$.

Throughout our work, we express scattering amplitudes as an expansion in the bare coupling constant α_B ,

$$\mathcal{A}_B = \sum_{l=0}^n \left(\frac{\alpha_B}{2\pi}\right)^l \mathcal{A}_B^{(l)}, \quad (5)$$

where $\mathcal{A}_B^{(l)}$ is the bare amplitude at loop order l .

B. Tensor Decomposition

Using symmetries such as Lorentz and gauge invariance we can form a basis of tensor structures (\mathcal{T}_i) that comprise the scattering amplitudes we are considering. These tensor structures are built by accounting for the physical states of the (D -dimensional) external particles.

We can then break the amplitudes down into form factors, that are completely independent of states of the external particles, which correspond to these tensor structures. We can then construct the scattering amplitude by summing the products of form factors and their corresponding tensor structures,

$$\mathcal{A}_B^{(l)} = \sum_{i=1}^n \mathcal{F}_{B;i}^{(l)} \mathcal{T}_i^{(l)}, \quad (6)$$

where $\mathcal{F}_{B;i}^{(l)}$ and $\mathcal{T}_i^{(l)}$ are the form factors and tensor structures at a given loop order l .

In summary, tensor decomposition allows us to express scattering amplitudes as form factors comprised of scalar products of external and loop momenta. These expressions can be simplified to sums of scalar integrals, whilst encapsulating the complexity of spinors and polarisation vectors within the tensor structures, which we can treat as four-dimensional, and introduce in the final stages of the calculation. This method is not only beneficial for the purposes of this paper, where we compute helicity amplitudes, but can also be used to compute the interference of scattering amplitudes at loop level.

To obtain these form factors from an amplitude we build a projector operator from the relevant tensor structures. To build this projector operator, we first form a matrix,

$$M_{ij}^{(l)} = \mathcal{T}_i^{(l)\dagger} \mathcal{T}_j^{(l)}. \quad (7)$$

Then, using this matrix, we obtain the projector operator via,

$$\mathcal{P}_i^{(l)} = \sum_j \left(M_{ij}^{(l)} \right)^{-1} \mathcal{T}_j^{(l)}, \quad (8)$$

which, when applied onto the amplitude, gives us the form factors,

$$\mathcal{F}_{B;i}^{(l)} = \mathcal{P}_i^{(l)} \mathcal{A}_B^{(l)}. \quad (9)$$

Referring back to Eq. (6), we can see that the only dependence on the configuration of the external states resides within the tensor structures \mathcal{T}_i , which have until now been considered in D space-time dimensions. For the purpose of our following calculations, however, we are interested in computing physical quantities in $D = 4$. We can benefit from this as we can relate tensor structures with independent helicity configurations of the amplitudes. This scheme is very similar to the 't Hooft-Veltman scheme, where internal states are considered in D dimensions and external states are considered in four dimensions.

In essence, we perform all of the gamma algebra, Lorentz contractions and compute traces in D dimensions when we are constructing our form factors $\mathcal{F}_{B;i}^{(l)}$ thereby confining all of the D -dimensional dependence to them. Whereas we can specify the tensor structures

\mathcal{T}_i to be in four dimensions when we fix the helicities of the external states. This corresponds to the dimensional regularisation scheme used in [33].

This has the benefit of reducing the number of form factors we need to consider. Said differently, some tensor structures that are independent in D dimensions become dependent once we restrict them to the four-dimensional space of external momenta. Therefore, these tensor structures are valid at all loop orders and we can safely drop their superscript (l) in Eq. (6) to only refer to four-dimensional physical processes.

C. Matrix-Based Method for Grouping Feynman Diagrams

Integration-by-parts (IBP) relations, which will be discussed in Sec. II D, are extremely useful in the calculation of scattering amplitudes. However, they can be a bottleneck in many calculations. Hence, it is beneficial to reduce the number of IBP relations we have to find. One way to do this is to group diagrams that obey the same IBP relations. In order to achieve this, we need to find diagrams that share propagators. This isn't always immediately obvious as there are multiple ways that we can assign momenta to Feynman diagrams. Therefore, we not only need to consider diagrams that share propagators, but also those that share propagators after a shift in the loop momenta. This can be a challenging task due to the vast amount of loop momenta shifts that are possible.

For instance, at two loops, if we consider a traditional method in which we check every possible shift to see if a match is possible, the number of possible momenta shift permutations that would need to be considered is 59,049. This would be for a case where we know which "Parent" diagram a sub-diagram will match to. However, if we consider a case where we don't know which "Parent" diagram a sub-diagram would map to, then we would need to compare each sub-diagram to many diagrams increasing the permutations we need to consider further. Therefore, we need an efficient method to find these groupings of diagrams, and the momenta shift required to obtain matching propagators.

We opt for a method to represent the propagators for each diagram as a matrix. Then, through matrix manipulations, we are able to find the possible momenta shifts to obtain matching propagators.

Matrix Representation of Feynman diagrams

The idea is that each row of the matrix represents a propagator. For example,

$$(p_2 + p_3 - q_2)^2 \rightarrow \{0, -1, 1, 1, 0\}, \quad (10)$$

where each column in the row corresponds to q_1, q_2, p_2, p_3, p_4 respectively.

Once we have done this for each propagator we represent all propagators in a matrix form,

$$\frac{1}{(q_1)^2(q_2)^2(q_1+q_2)^2(p_4-q_2)^2(p_3+q_1+q_2)^2} \times \frac{1}{(p_2+p_3+q_1+q_2)^2(p_2+p_3+p_4+q_1)^2} \downarrow \begin{pmatrix} -1 & 0 & 0 & 0 & 0 \\ 0 & -1 & 0 & 0 & 0 \\ -1 & -1 & 0 & 0 & 0 \\ 0 & -1 & 0 & 0 & 1 \\ -1 & -1 & 0 & -1 & 0 \\ -1 & -1 & -1 & -1 & 0 \\ -1 & 0 & -1 & -1 & -1 \end{pmatrix}, \quad (11)$$

where we have ensured that all instances of the loop momenta are negative. In the next section, we discuss how we can use these matrices to find momenta shifts between diagrams.

Although we limit the presentation of our method in this section to the grouping of Feynman diagrams with massless propagators, this representation can be extended to account for massive propagators by simply adding additional columns for the internal masses involved in the process.

Finding Momenta Shifts

The next step is to find the momenta shifts of diagrams with fewer than 7 unique propagators that will make their propagators align with a parent diagram's. To achieve this, we compare the rows of a sub-diagram's matrix, after an arbitrary shift, to that of a parent diagram.

Firstly, let us consider how to represent a shifted matrix. When we shift the loop momenta q_1 and q_2 , we end up with,

$$\begin{aligned} q_1 &\rightarrow aq_1 + bq_2 + cp_2 + dp_3 + ep_4, \\ q_2 &\rightarrow fq_1 + gq_2 + hp_2 + ip_3 + jp_4, \end{aligned} \quad (12)$$

where $a, b, c, d, e, f, g, h, i, j \in \{-1, 0, 1\}$.

In matrix form, this shift becomes,

$$\begin{pmatrix} q_1 \\ q_2 \\ p_2 \\ p_3 \\ p_4 \end{pmatrix} \rightarrow \begin{pmatrix} a & b & c & d & e \\ f & g & h & i & j \\ 0 & 0 & 1 & 0 & 0 \\ 0 & 0 & 0 & 1 & 0 \\ 0 & 0 & 0 & 0 & 1 \end{pmatrix} \cdot \begin{pmatrix} q_1 \\ q_2 \\ p_2 \\ p_3 \\ p_4 \end{pmatrix}. \quad (13)$$

Here and in the following, we refer to this matrix as the "Shift Matrix"¹. We then produce a matrix that consists

of the coefficients of the shifted loop momenta by multiplying a diagram's matrix representation, for example Eq. (11), by the Shift Matrix.

We can then set up systems of linear equations² by comparing the elements of the shifted diagram with those of a parent diagram. This could appear problematic as a diagram with fewer propagators will have fewer rows to their matrix, so we cannot make a comparison with a parent matrix. To account for this, we make the comparisons with permutations of the rows of the parent matrix. For example, if we want to find the shift of a diagram with 5 propagators to a parent with 7 propagators, we consider all of the permutations of 5 rows of the parent matrix, and then try to solve the system of linear equations for the variables $\{a, b, c, \dots, j\}$. If we find a solution to a system of equations, we have found a possible shift from a sub-diagram to a parent diagram. We opted to solve this system of equations analytically, however numerical methods could also be applied.

This method reduces the amount of permutations that we have to consider, as we are only considering permutations of rows of a matrix, rather than considering every possible expression that each loop momenta could take after a shift. In the two-loop case, if we consider a traditional method to find the momenta shifts for the two loop momenta, we have 10 variables $\{a, b, c, \dots, j\}$ that can each take the values $\{-1, 0, 1\}$. Therefore, we have $3^{10} = 59,049$ possible permutations of loop momenta shifts for every sub-diagram. However, using the matrix-based method that we have proposed, we can reduce the permutations that need to be considered to $\frac{7!}{(7-6)!} = 5,040$ for diagrams with 6 propagators, $\frac{7!}{(7-5)!} = 2,520$ for diagrams with 5 propagators, and $\frac{7!}{(7-4)!} = 840$ for diagrams with 4 propagators³.

In general, the number of permutations that need to be considered, when comparing against one parent diagram, can be calculated using,

$$\text{Permutations} = \frac{(N_{\text{parent}})!}{(N_{\text{parent}} - N_{\text{sub}})!}, \quad (14)$$

where N_{parent} and N_{sub} correspond to the number of propagators in the parent diagrams and sub-diagrams respectively.

The grouping of diagrams that we find after applying this method to the $e^+e^- \rightarrow \mu^+\mu^-$ and $e^+e^- \rightarrow \gamma\gamma$ processes can be found in Appendix A.

This method can be applied to massive cases and higher-loop orders as long as all parameters are accounted

¹ This Shift Matrix can also be extended to crossing of external kinematics, where additional requirements as momentum conservation and on-shell conditions need to be satisfied. This is considered with exchanges of external momenta by replacing the identity matrix in the external momentum columns/rows with arbitrary constants.

² In the two-loop case that we present, we have a system of 25 equations including 10 variables.

³ These values are how many permutations have to be considered when checking against one potential parent diagram. To check for shifts against all parent diagrams, we need to multiply these values by the amount of parent diagrams there are for the process.

for in the shift matrix. Whilst this is a novel approach, alternative methods to group Feynman diagrams into topological families have been suggested previously by using Symanzik polynomials in [40–43].

D. Reduction to Master Integrals

Reduction to scalar integrals

Once we decompose our amplitudes, that have been generated diagrammatically using FEYNALC [42] and FEYNARTS [44], into form factors, we obtain expressions that are a sum of integrands. These integrands contain scalar products of the loop momenta q_i and external momenta p_i in the numerator. However, in order to compute analytical expressions for the integrands in our form factors it is beneficial to express them as sum of scalar integrals of the form,

$$j(\text{fam}, \{a_1, a_2, \dots, a_N\}) = s^{-l\epsilon} e^{l\epsilon\gamma_E} \prod_{j=1}^l \int \left(\frac{d^D q_j}{i\pi^{D/2}} \right) \frac{1}{D_1^{a_1} D_2^{a_2} \dots D_N^{a_N}}, \quad (15)$$

where D_i are the inverse propagators of the internal particles, ‘fam’ is the integral family that the scalar integral belongs to, l denotes the number of loops that appear in the Feynman diagram we are considering, a_1, a_2, \dots, a_N are the powers on the denominators D_1, D_2, \dots, D_N and γ_E is the Euler-Mascheroni constant.

To go from our integrands to scalar integrals, we need to remove all dependence on scalar products of momenta in the numerator. To do this we need to find ways of expressing all of the scalar products in the numerator as linear combinations of the inverse propagators $\{D_i\}$. Depending on the loop order, this can require additional inverse propagators that do not appear in the original integrand expressions. We refer to these additional propagators as auxiliary propagators⁴. Take the example of the two-loop case, we will have D_1, D_2, \dots, D_7 as the internal propagators of the Feynman diagram, but we require two additional propagators D_8, D_9 in order to express all scalar products in terms of propagators. Once we have replaced the scalar products with propagators, every term in the expression can then be written as a product of the propagators $\{D_i\}$ to some power as seen in Eq. (15).

Upon expressing our form factors as a sum of scalar integrals, the next required step is to compute these integrals. However, this can become a bottleneck in the calculation. A useful technique to assist in these computations is integration-by-parts reduction.

⁴ As we have applied momenta shifts to group Feynman diagrams into families, we are able to choose auxiliary propagators that are sufficient for the whole family of diagrams rather than each diagram individually.

Integration-by-Parts Reduction

Once we have produced expressions for the form factors in terms of scalar integrals, we then begin to compute these integrals. However, given the multitude of scalar integrals that appear in our form factors, this can be quite a cumbersome task. We utilise the Laporta algorithm [16] to find integration-by-parts relations between integrals, so that we can express a large basis of integrals in terms of a minimal basis of “Master Integrals” (MIs). We opt to use the implementation of this algorithm in the MATHEMATICA package LITERED [45] to generate the IBP relations between integrals and MIs. We can then use the package FINITEFLOW [46] to speedily perform the reduction of form factors to MIs using analytical reconstructions over finite fields [47, 48].

E. Canonical Basis

Whilst performing our IBP reduction, we opt to use a canonical basis of master integrals [14]. We consider integrals that admit a $d \log$ representation [37]. Feynman integrands that admit a $d \log$ can be represented as differential forms, exhibiting a dx/x behaviour in each variable near singularities. Explicitly,

$$\mathcal{I}^{(l)} = \sum_{k=1}^{l|D|} c_k d \log \alpha_1^{(k)} \wedge d \log \alpha_2^{(k)} \wedge \dots \wedge d \log \alpha_n^{(k)}, \quad (16)$$

with,

$$d = \sum_{i=1}^n dx_i \frac{\partial}{\partial x_i}, \quad (17)$$

$\alpha_i^{(k)}$ represent the variables we are integrating over, and the wedge is the usual definition of a differential form giving rise to an oriented volume after integration. The coefficient c_k are the leading singularities of the integrand.

We obtain integrals that admit a $d \log$ representation using the package DLOGBASIS [37]. These integrals automatically obey the system of differential equations in canonical form,

$$d\mathbf{g}(s, t; \epsilon) = \epsilon d\tilde{\mathbf{A}} \cdot \mathbf{g}(s, t; \epsilon), \quad (18)$$

with,

$$\tilde{\mathbf{A}} = \sum_{k=1}^3 \mathbf{A}_k \log [W_k(s, t)], \quad (19)$$

where \mathbf{A}_k are \mathbb{Q} matrices, \mathbf{g} the basis of master integrals, and W_k represent the letters of the alphabet,

$$W_1 = s, \quad W_2 = t, \quad W_3 = u = -s - t. \quad (20)$$

With the canonical differential equation (18), we can express our sets of master integrals as,

$$\mathbf{g}(s, t; \epsilon) = \mathbb{P} \exp \left(\epsilon \int_c d\tilde{\mathbf{A}} \right) \mathbf{g}_0(\epsilon), \quad (21)$$

where \mathbb{P} accounts for the path ordering in the matrix exponential along the contour \mathcal{C} in the space of the kinematic variables s, t , and \mathbf{g}_0 represents the boundary values at the base point of the contour \mathcal{C} .

By assigning a transcendental weight of -1 to ϵ , we can choose a basis $\mathbf{g}(s, t; \epsilon)$ that has uniform transcendental weight, such that its expansion around $\epsilon = 0$ starts at order ϵ^0 ,

$$\mathbf{g}(s, t; \epsilon) = \sum_{w \geq 0} \epsilon^w \mathbf{g}^{(w)}(s, t), \quad (22)$$

where $\mathbf{g}^{(w)}(s, t)$ are the terms in the expansion of $\mathbf{g}(s, t; \epsilon)$ at transcendental weight w . For the purpose of the calculations in this work, we integrate our MIs up to transcendental weight six.

At one-loop, poles start at $\mathcal{O}(\epsilon^{-2})$ and at two-loop poles start at $\mathcal{O}(\epsilon^{-4})$. Expanding up to weight 6 gives expressions for the one-loop integrals up to ϵ^4 and two-loop integrals up to ϵ^2 .

In order to solve the differential equations (18), we need to provide boundary conditions at each order in ϵ . For the sake of the simplicity and to systematically account for analytic continuation of integrals, we use the package AMFLOW [49, 50] to evaluate our MIs phase-space points in the production region (3).

We express the analytical expressions for our MIs in terms of generalised polylogarithms (GPLs) [39] as function of the dimensionless variable x of Eq. (4). GPLs can be expressed as the recursively iterated integrals,

$$G(a_1, \dots, a_n; x) = \int_0^x \frac{dt}{t - a_1} G(a_2, \dots, a_n; t), \quad (23)$$

where at least one $a_i \neq 0$. We also define $G(; t) = 1$. The length of the vector $\vec{a} = (a_1, a_2, \dots, a_n)$ defines the transcendental weight of the GPL. In the case where all $a_i = 0$, we define,

$$G(0_1, 0_2, \dots, 0_n; x) = \frac{1}{n!} \log^n(x), \quad (24)$$

where n is the number of 0s.

We construct a minimal basis of GPLs up to transcendental weight six functions, by systematically enumerating Lyndon words on the sets $\{0, 1\}$ through the function `DecomposeToLyndonWords` of `POLYLOGTOOLS` [51]. This means that we are able to express all form factors in terms of at most 23 GPLs, which makes numerical evaluation of our final results more efficient.

One-Loop Canonical Basis

We can express all one-loop Feynman integrals within the scattering amplitudes in terms of 5 MIs. These integrals stem from the one-loop box shown in Fig. 2 and the diagram that results from exchanging the external legs with momenta p_3 and p_4 , which we will henceforth refer

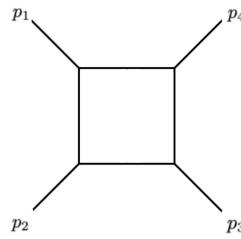


FIG. 2: One-loop box with the ordering of external momenta of Fig. 1.

Denominator	Propagator
D_1	$(q)^2$
D_2	$(q - p_2)^2$
D_3	$(q - p_2 - p_3)^2$
D_4	$(q - p_2 - p_3 - p_4)^2$

TABLE I: Propagators for the one-loop box of Fig. 2.

to as the “crossed box”. The complete set of propagators that are used to perform IBP reduction on these diagrams are seen in Table I. From this propagator configuration, we obtain 3 MIs which we shall denote as $d\log(1234, i)$, with $i = 1, 2, 3$. These MIs correspond respectively to the one-loop box in the (s, t) -channel, the one-loop triangle in the t -channel and the one-loop triangle in the s -channel.

To find the MIs that are obtained from the crossed box we can simply perform an exchange of p_3 and p_4 in the propagators, as well as performing an exchange of t and $u = -s - t$ in any kinematic pre-factors to the MIs produced by the one-loop box. These integrals will be denoted as $d\log(1243, i)$, where $i = 1, 2, 3$.

Altogether we have 6 canonical integrals, but due to Lorentz symmetries $d\log(1234, 3)$ is identical to $d\log(1243, 3)$ when p_3 and p_4 are exchanged. Therefore we are left with 5 canonical MIs.

Two-Loop Canonical Basis

At two-loop level, all integrals contained within the scattering amplitudes of both the $e^+e^- \rightarrow \mu^+\mu^-$ and $e^+e^- \rightarrow \gamma\gamma$ processes can be expressed in terms of MIs that are derived from two diagrams and permutations of their external momenta. This allows us to split the MIs into two cases, those that come from planar (PL) diagrams and those that come from non-planar (NPL) diagrams.

Let us consider the planar and non-planar diagrams that have the external momenta configuration of Fig. 1 that can be seen in Fig. 3. The complete set of propagators D_i that are used to perform the IBP reduction for these diagrams are summarised in Table II.

The planar diagram shown above provides 8 MIs that

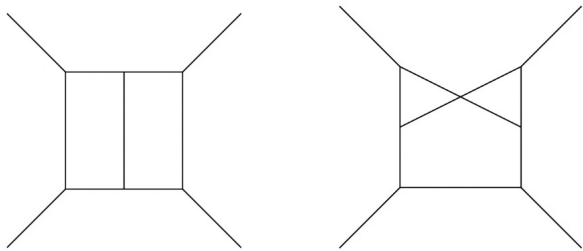


FIG. 3: The two-loop topologies that define our planar (PL) and non-planar (NPL) integral families.

Diagram	PL	NPL
D_1	$(q_1)^2$	$(q_1)^2$
D_2	$(q_1 - p_2 - p_3 - p_4)^2$	$(q_1 - p_2 - p_3 - p_4)^2$
D_3	$(q_1 - p_3 - p_4)^2$	$(p_4 - q_1 + q_2)^2$
D_4	$(q_2)^2$	$(q_2)^2$
D_5	$(q_2 - p_3 - p_4)^2$	$(q_2 - p_2 - p_3)^2$
D_6	$(q_2 - p_4)^2$	$(q_2 - p_3)^2$
D_7	$(q_1 - q_2)^2$	$(-q_1 + q_2)^2$
D_8	$(q_1 - p_4)^2$	$(q_1 - p_3)^2$
D_9	$(q_2 - p_2 - p_3 - p_4)^2$	$(q_2 - p_2 - p_3 - p_4)^2$

TABLE II: Propagators for planar and non-planar diagrams in the configuration of external momenta of Fig. 1.

we denote by $d\log(\text{PL}1234, i)$, where $i = 1, 2, 3, \dots, 8$. Similarly, the non-planar diagram shown above provides 12 MIs that we denote by $d\log(\text{NPL}1234, i)$, where $i = 1, 2, 3, \dots, 12$.

If we are to consider just these two diagrams, we will not have a sufficient basis to express all integrals in terms of MIs. Therefore, we must also consider the permutations of the external momenta. If we fix p_1 in its position and permute the remaining external momenta we create six families each for both the planar and the non-planar cases.

Let us consider the case where the external momenta configuration in which p_2 and p_3 have been exchanged, as seen in Fig. 4. This diagram will produce an additional 8 canonical integrals. It is possible to derive these MIs from the basis $d\log(\text{PL}1234, i)$ by simply exchanging p_2 with p_3 in each of the propagators shown in Table II as well as performing the exchange of s and $u = -s - t$ in the kinematical pre-factors. We denote these MIs as $d\log(\text{PL}1324, i)$, with $i = 1, 2, 3, \dots, 8$.

Repeating this process for all possible permutations of both the planar and non-planar case gives us 120 integrals. We then look to see if any of these integrals have symmetries or relations to each other. We prioritise planar integrals over non-planar integrals. Once we have considered relations and symmetries between these integrals we are able to express all integrals in terms of a minimal set of at most 39 MIs. Further details on the

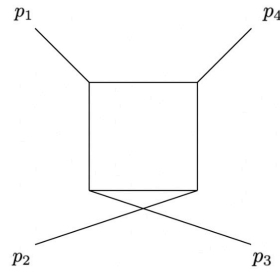


FIG. 4: Two-loop planar diagram with an exchange of p_2 and p_3 .

MIs for the two-loop $e^+e^- \rightarrow \mu^+\mu^-$ and $e^+e^- \rightarrow \gamma\gamma$ processes can be found in Appendix B.

III. UV RENORMALISATION AND IR SUBTRACTION

Once we have expressed our form factors as an expansion in the bare coupling constant (5), we obtain expressions that contain ϵ poles in the dimensional regulator.⁵ In this section we discuss the techniques we use to remove these poles.

The singularities in our expressions appear in two forms: UV and IR divergences. UV divergences are due to divergences in the integrals when loop momenta become infinite, whereas IR divergences stem from the soft emissions and collinear singularities. We will first address how we remove the UV poles, followed by the IR poles.

To maintain a general perspective in this section, we will refer to scattering amplitudes. This approach is valid since both UV renormalization and IR subtraction can be applied to scattering amplitudes and form factors in a similar manner.

A. UV Renormalisation

We absorb UV divergences by renormalising the couple constant in the $\overline{\text{MS}}$ scheme. In detail, we exchange bare with a renormalised coupling constant as follows,

$$\alpha_B \mu_0^{2\epsilon} S_\epsilon = \alpha \mu^{2\epsilon} \times \left[1 - \frac{\beta_0}{\epsilon} \left(\frac{\alpha}{2\pi} \right) + \left(\frac{\beta_0^2}{\epsilon^2} - \frac{\beta_1}{2\epsilon} \right) \left(\frac{\alpha}{2\pi} \right)^2 + \mathcal{O}(\alpha^3) \right], \quad (25)$$

where α is the renormalised coupling constant, μ is the renormalisation scale, $S_\epsilon = \exp(-\epsilon\gamma_E)$ is the normalisation factor. Additionally, we have the β functions,

$$\beta_0 = -\frac{2N_f}{3} \text{ and } \beta_1 = -N_f, \quad (26)$$

⁵ We can also apply the same renormalisation techniques directly on bare scattering amplitudes \mathcal{A}_B .

with N_f the number of fermions.

After performing the exchange and re-writing our amplitudes as an expansion in $(\frac{\alpha}{2\pi})$, we can find the renormalised l -loop amplitudes by considering the coefficient of $(\frac{\alpha}{2\pi})^{(l)}$. From this we obtain the following relations between the bare amplitudes and the renormalised amplitudes,

$$\mathcal{A}^{(0)} = \mathcal{A}_B^{(0)}, \quad (27a)$$

$$\mathcal{A}^{(1)} = \mathcal{A}_B^{(1)} - \frac{\beta_0}{\epsilon} \mathcal{A}_B^{(0)}, \quad (27b)$$

$$\mathcal{A}^{(2)} = \mathcal{A}_B^{(2)} - \frac{2\beta_0}{\epsilon} \mathcal{A}_B^{(1)} + \left(\frac{\beta_0^2}{\epsilon^2} - \frac{\beta_1}{2\epsilon} \right) \mathcal{A}_B^{(0)}, \quad (27c)$$

where $\mathcal{A}^{(l)}$ are the l -loop renormalised amplitudes.

When we substitute the expressions for our bare amplitudes into these equations, we obtain the renormalised amplitudes that contain no UV poles.

B. IR Subtraction

Once we have expressions for our renormalised amplitudes, we can now remove the remaining poles using IR subtraction in the Soft-Collinear Effective Theory (SCET) formalism [52].

We should note that we have utilised techniques that are relevant in QCD to obtain many of the expressions required to remove the remaining poles. We then abelianise these expressions to get the relevant expressions for our QED processes. Therefore, our derivations may include terminology relevant in QCD rather than QED.

The finite remainder of an amplitude can be written as,

$$\mathcal{R}(\{p\}, \mu) = \lim_{\epsilon \rightarrow 0} \mathcal{Z}^{-1}(\epsilon, \{p\}, \mu) \mathcal{A}(\epsilon, \{p\}), \quad (28)$$

where \mathcal{Z} is the multiplicative colour-space operator.

We can apply this at each loop order to obtain the following relations:

$$\mathcal{R}^{(0)} = \mathcal{A}^{(0)}, \quad (29a)$$

$$\mathcal{R}^{(1)} = \mathcal{A}^{(1)} - \mathcal{I}^{(1)} \mathcal{A}^{(0)}, \quad (29b)$$

$$\mathcal{R}^{(2)} = \mathcal{A}^{(2)} - \mathcal{I}^{(1)} \mathcal{A}^{(1)} - \mathcal{I}^{(2)} \mathcal{A}^{(0)}, \quad (29c)$$

where $\mathcal{I}^{(n)}$ are the subtraction operators,

$$\mathcal{I}^{(1)} = \mathcal{Z}^{(1)}, \quad (30a)$$

$$\mathcal{I}^{(2)} = \mathcal{Z}^{(2)} - \left(\mathcal{Z}^{(1)} \right)^2. \quad (30b)$$

The expressions for $\mathcal{Z}^{(m)}$ operators themselves can be found by solving the equation,

$$\mathcal{Z}(\epsilon, \{p\}, \mu) = \mathbb{P} \exp \left[\int_{\mu}^{\infty} \frac{d\mu'}{\mu'} \Gamma(\{p\}, \mu) \right]. \quad (31)$$

In this equation, the anomalous dimension matrix Γ is defined as,

$$\Gamma = \Gamma_{\text{dipole}}(\{p\}, \mu) + \Delta_4, \quad (32)$$

where Γ_{dipole} corresponds to the colour dipole correlations and Δ_4 contains the quadrupole colour correlations.

Once we have abelianised our expressions, Δ_4 vanishes. Therefore, we only need to consider Γ_{dipole} in this work. We will refer to Γ_{dipole} as Γ from this point onwards.

The explicit expression for the anomalous dimension Γ reads as,

$$\Gamma(\{p\}, \mu) = \sum_{1 \leq i < j \leq n} T_i^a T_j^a \gamma^{\text{cusp}} L_{ij} + \sum_i^n \gamma^i, \quad (33)$$

with,

$$L_{ij} = \log \left(\frac{\mu^2}{-s_{ij} - i0} \right), \quad (34)$$

s_{ij} are Mandelstam invariants,

$$s_{12} = s_{34} = s, \quad s_{23} = s_{14} = t, \quad \text{and} \quad s_{13} = s_{24} = u, \quad (35)$$

and T_i^a are the generators of the $\text{SU}(N_c)$ group, associated with the particle i . The second term in Eq. (33) is dependent on the external particles in the process. Therefore, Γ differs when we consider different processes. These generators are written in terms of the Casimir invariants C_A and C_F . Because we are focused on QED processes, we abelianise by setting $C_A \rightarrow 0$ and $C_F \rightarrow 1$, and $T_i \rightarrow q_i$, corresponding to the charge of the i -th external particle.

In Eq. (33), γ^{cusp} is the cusp anomalous dimension coefficient and γ^i is the anomalous dimension coefficient for particle i .

Additionally, the IR renormalisation factor Z_{IR} is defined by the exponentiation of,

$$\log Z_{\text{IR}} = \sum_{k=1}^l \left(\frac{\alpha}{2\pi} \right)^k \mathcal{Z}^{(k)}. \quad (36)$$

with

$$\mathcal{Z}^{(1)} = \frac{\Gamma'_0}{4\epsilon^2} + \frac{\Gamma_0}{2\epsilon}, \quad (37a)$$

$$\begin{aligned} \mathcal{Z}^{(2)} = & \frac{\Gamma_0'^2}{32\epsilon^4} + \frac{\Gamma_0}{8\epsilon^3} \left(\Gamma_0 - \frac{3}{2}\beta_0 \right) \\ & + \frac{1}{4\epsilon^2} \left(-\beta_0 \Gamma_0 + \frac{\Gamma_0^2}{2} + \frac{\Gamma_1'}{4} \right) + \frac{\Gamma_1}{4\epsilon}. \end{aligned} \quad (37b)$$

By substituting the corresponding anomalous dimension coefficients for the relevant process, which can be found in Appendix C, and performing the IR subtraction, we are able to remove all remaining divergences and obtain expressions for our processes that are of $\mathcal{O}(\epsilon^0)$ or higher. This cancellation of IR poles serves as a consistency check, as it confirms that the structure predicted by lower loop orders is indeed reproduced through direct calculation.

IV. RESULTS

In this section, we shall use our results from the computation of form factors to present the helicity amplitudes, for non-vanishing helicity configurations, for all processes (1). Additionally, we present the bare one-loop form factors, in terms of integrals, for the $e^+e^- \rightarrow \mu^+\mu^-$ and the $e^+\mu^- \rightarrow e^+\mu^-$ scatterings to illustrate how we can exchange momenta to obtain results for different processes. Expressions for the one- and two-loop form factors for the $e^+e^- \rightarrow \mu^+\mu^-$, $e^+\mu^- \rightarrow e^+\mu^-$ and $e^+e^- \rightarrow \gamma\gamma$ processes can be found in the ancillary files. We do not provide the bare form factors for $e^+e^- \rightarrow e^+e^-$ as we obtain the helicity amplitudes for this process from the form factors of $e^+e^- \rightarrow \mu^+\mu^-$ and $e^+\mu^- \rightarrow e^+\mu^-$ after UV renormalisation and IR subtraction.

At this stage we opt to introduce the dimensionless variable x (4), which roughly corresponds to setting $s = 1$, and allows to reduce the alphabet (20) to two letters, $\{x, 1-x\}$. The dependence on s is easily recovered by dimensional analysis.

Furthermore, we introduce an additional subscript to the form factors \mathcal{F}_i to help us distinguish between the processes:⁶

- $\mathcal{F}_{\mu\mu,i}$ for $e^+e^- \rightarrow \mu^+\mu^-$.
- $\mathcal{F}_{e\mu,i}$ for $e^+\mu^- \rightarrow e^+\mu^-$.
- $\mathcal{F}_{\gamma\gamma,i}$ for $e^+e^- \rightarrow \gamma\gamma$.

We introduce a similar notation for the tensor structures \mathcal{T}_i .

We find that for processes involving four fermions we obtain expressions for the form factors and helicity amplitudes that take the form:

$$\begin{aligned} \text{Tree-Level} &\sim A_{f_3 f_4}^{(0)}, \\ \text{One-Loop} &\sim A_{f_3 f_4}^{(1)} + N_f B_{f_3 f_4}^{(1)}, \\ \text{Two-Loop} &\sim A_{f_3 f_4}^{(2)} + N_f B_{f_3 f_4}^{(2)} + N_f^2 C_{f_3 f_4}^{(2)}, \end{aligned} \quad (38)$$

where f_i is the flavour of the fermion with momenta p_i .

Similarly, for $e^+e^- \rightarrow \gamma\gamma$ we find that the form factors and helicity amplitudes take the form:

$$\begin{aligned} \text{Tree-Level} &\sim A_{\gamma\gamma}^{(0)}, \\ \text{One-Loop} &\sim A_{\gamma\gamma}^{(1)}, \\ \text{Two-Loop} &\sim A_{\gamma\gamma}^{(2)} + N_f B_{\gamma\gamma}^{(2)}. \end{aligned} \quad (39)$$

A. $e^+e^- \rightarrow \mu^+\mu^-$

For the $e^+e^- \rightarrow \mu^+\mu^-$ scattering there are 2 independent Lorentz structures that can appear when we consider the external momenta to be in four space-time dimensions,

$$\begin{aligned} T_{\mu\mu,1} &= \bar{u}(p_2)\gamma_\mu u(p_1) \times \bar{u}(p_4)\gamma^\mu u(p_3), \\ T_{\mu\mu,2} &= \bar{u}(p_2)\not{p}_3 u(p_1) \times \bar{u}(p_4)\not{p}_1 u(p_3). \end{aligned} \quad (40)$$

Using the techniques outlined in Sec. II B, we can construct projectors to obtain the tensor decomposition for this process.

For these tensor structures there are 4 non-vanishing helicity configurations:

$$\{-++-, -+-+, +---, +-+-\}. \quad (41)$$

In our results, we shall present the helicity amplitudes of the first two configurations, as the latter two can be obtained by applying parity to these helicity configurations. We achieve this by taking the complex conjugate of these configurations.

To form an expression for the helicity amplitude from the form factors, we need to find a consistent representation for the tensor structures. Using spinor helicity formalism [53], we can express both tensor structures in the form of:

$$\{\Phi_{\mu\mu,(-+++)}, \Phi_{\mu\mu,(-++-)}\} = \{\langle 14 \rangle [23], \langle 13 \rangle [24]\}. \quad (42)$$

Expressing the tensor structures in these forms introduces pre-factors in terms of the Mandelstam variables to our form factors. Specifically, to obtain the helicity amplitudes for our two configurations, we need to sum our form factors as,

$$\begin{aligned} \mathcal{H}_{\mu\mu,(-+++)}^{(l)} &= -2\mathcal{F}_{\mu\mu,1}^{(l)} + (1-x)\mathcal{F}_{\mu\mu,2}^{(l)}, \\ \mathcal{H}_{\mu\mu,(-++-)}^{(l)} &= -2\mathcal{F}_{\mu\mu,1}^{(l)} - x\mathcal{F}_{\mu\mu,2}^{(l)}. \end{aligned} \quad (43)$$

We then multiply these expressions by their corresponding spinor structures,

$$\mathcal{A}_{\mu\mu,(\lambda_1\lambda_2\lambda_3\lambda_4)}^{(l)} = \mathcal{H}_{\mu\mu,(\lambda_1\lambda_2\lambda_3\lambda_4)}^{(l)} \Phi_{\mu\mu,(\lambda_1\lambda_2\lambda_3\lambda_4)}, \quad (44)$$

where λ_i corresponds to the helicity of the i -th external particle with momentum p_i . These expressions for the helicity amplitudes, in terms of form factors, are valid at all loop orders.

⁶ These form factors have undergone UV renormalisation and IR subtraction, thus will contain no poles.

One-Loop bare form factors

Here we present the one-loop bare form factors, $\mathcal{F}_{B;\mu\mu,i}^{(1)}$,⁷ in terms of master integrals,

$$\begin{aligned} \mathcal{F}_{B;\mu\mu,1}^{(1)} = & \frac{1}{2\epsilon^2(1-2\epsilon)s} \left[d\log(1234, 1) \left(\frac{\epsilon s - 2s - 4\epsilon u}{2u} \right) + d\log(1234, 2) \left(\frac{2s - \epsilon s - 2u(\epsilon - 2)}{u} \right) \right. \\ & \left. + d\log(1234, 3) \left(\xi \left((2\epsilon^2 - \epsilon + 2) + \frac{2\epsilon(\epsilon - 1)}{(2\epsilon - 3)} N_f \right) - \frac{(\epsilon - 2)s}{u} \right) \right] - \{p_3 \leftrightarrow p_4, \xi \rightarrow -\xi\}, \end{aligned} \quad (45)$$

we then must set $\xi = 1$.

$$\begin{aligned} \mathcal{F}_{B;\mu\mu,2}^{(1)} = & \frac{1}{\epsilon^2(1-2\epsilon)tu} \left[-d\log(1234, 1) \left(\frac{\epsilon^2 s^2 - \epsilon st - 4\epsilon t^2 + 2st + 4t^2}{2su} \right) \right. \\ & \left. + d\log(1234, 2) \frac{(2\epsilon^2 s^2 + \epsilon^2 st + \epsilon st - 2\epsilon t^2 + 2st + 4t^2)}{su} + d\log(1234, 3) \left((4 - 6\epsilon + \epsilon^2) + \frac{(\epsilon - 2)(\epsilon - 1)s}{u} \right) \right] \\ & + \{p_3 \leftrightarrow p_4\}. \end{aligned} \quad (46)$$

The exchange of p_3 and p_4 in both form factors implies the exchange of t and u .

Let us first discuss the integrals that are part of the family 1234,

$$\begin{aligned} d\log(1234, 1) &= \epsilon^2 st j(1234, \{1, 1, 1, 1\}), \\ d\log(1234, 2) &= \epsilon^2 t j(1234, \{1, 1, 1, 0\}), \\ d\log(1234, 3) &= \epsilon^2 s j(1234, \{1, 1, 0, 1\}). \end{aligned} \quad (47)$$

The denominators for this family of integrals can be found in Table I. We are able to obtain the integrals that are part of the family 1243 as follows:

$$d\log(1243, i) = d\log(1234, i) \Big|_{p_3 \leftrightarrow p_4}, \quad (48)$$

for $i = 1, 2, 3$. The denominators for this family of integrals can be found by exchanging p_3 and p_4 in the denominators presented in Table I.

Two-Loop bare form factors

The two-loop bare form factors for $e^+e^- \rightarrow \mu^+\mu^-$ are provided in the ancillary files. These form factors consist of the two-loop integrals discussed in Sec. II E.

Similarly to the one-loop case, we are able to obtain the MIs for two of these integral families: PL1234 and NPL1234. Then we can perform swaps of external momenta to obtain the master integrals for the remaining families. For example:

$$d\log(\text{PL1243}, i) = d\log(\text{PL1234}, i) \Big|_{p_3 \leftrightarrow p_4}, \quad (49)$$

for $i = 1, 2, 3, \dots, 8$. Also,

$$d\log(\text{NPL1243}, i) = d\log(\text{NPL1234}, i) \Big|_{p_3 \leftrightarrow p_4}, \quad (50)$$

for $i = 1, 2, 3, \dots, 12$.

Additional information about the two-loop integral families required for the $e^+e^- \rightarrow \mu^+\mu^-$ can be found in Appendix B.

B. $e^+\mu^- \rightarrow e^+\mu^-$

As we are considering the massless case for each process, the $e^+\mu^- \rightarrow e^+\mu^-$ scattering amplitude may be derived directly from the $e^+e^- \rightarrow \mu^+\mu^-$ as both processes consider a four fermion $2 \rightarrow 2$ scattering.

Compared to the $e^+e^- \rightarrow \mu^+\mu^-$ scattering, the flavours of the particles with momenta p_2 and p_4 are swapped. Therefore, to obtain the form factors at all loop levels for the $e^+\mu^- \rightarrow e^+\mu^-$ we can simply exchange the momenta p_2 and p_4 . This exchange leads to several changes to our expressions. Firstly, we must

⁷ We have added the subscript B to clarify that these are expressions for the bare form factors.

swap the Mandelstam variables s and t . Secondly, after swapping the external momenta, the propagators in the integrals will also change. Therefore, we must perform an exchange of p_2 and p_4 on the integral families in our expressions before computing them.

There are 4 non-vanishing helicity configurations for this process,

$$\{- - ++, - + - +, + + --, + - + -\}. \quad (51)$$

Similarly to the $e^+e^- \rightarrow \mu^+\mu^-$ process, in our results we present helicity amplitudes for the first two configurations,

$$\{\Phi_{e\mu,(- - ++)}, \Phi_{e\mu,(- + - +)}\} = \{\langle 12 \rangle [34], \langle 13 \rangle [24]\}. \quad (52)$$

To obtain the corresponding helicity amplitudes for these configurations we need to sum the form factors with the following pre-factors:

$$\mathcal{H}_{e\mu,(- - ++)}^{(l)} = 2\mathcal{F}_{e\mu,1}^{(l)} - (1-x)\mathcal{F}_{e\mu,2}^{(l)},$$

$$\begin{aligned} \mathcal{F}_{B;e\mu,1}^{(1)} &= \frac{1}{2\epsilon^2(1-2\epsilon)t} \left[d\log(1432, 3) \left(\xi \left((2-\epsilon+2\epsilon^2) + \frac{2\epsilon(\epsilon-1)}{2\epsilon-3} N_f \right) - \frac{(\epsilon-2)t}{u} \right) \right. \\ &\quad \left. + \frac{1}{2} d\log(1432, 1) \left((2-5\epsilon) - \frac{(\epsilon-2)s}{u} \right) + d\log(1432, 2) (2-\epsilon) \left(1 - \frac{s}{u} \right) \right] - \{p_2 \leftrightarrow p_3, \xi \rightarrow -\xi\}, \end{aligned} \quad (57)$$

we then must set $\xi = 1$.

$$\begin{aligned} \mathcal{F}_{B;e\mu,2}^{(1)} &= -\frac{1}{\epsilon^2(1-2\epsilon)su} \left[-d\log(1432, 3) \left(\frac{t(\epsilon^2-3\epsilon+2)}{u} + (4-6\epsilon+\epsilon^2) \right) \right. \\ &\quad \left. + d\log(1432, 1) \left(\frac{\epsilon^2 t^2 - 4\epsilon s^2 - \epsilon st + 4s^2 + 2st}{2tu} \right) - d\log(1432, 2) \left(\frac{\epsilon^2 st + 2\epsilon^2 t^2 - 2\epsilon s^2 + \epsilon st + 4s^2 + 2st}{tu} \right) \right] + \{p_2 \leftrightarrow p_3\}. \end{aligned} \quad (58)$$

Let us discuss the integrals that are part of the families 1432 and 1423. The integrals in these families can be found by considering the following exchange of external momenta,

$$\begin{aligned} d\log(1432, i) &= d\log(1234, i) \Big|_{p_2 \leftrightarrow p_4}, \\ d\log(1423, i) &= d\log(1243, i) \Big|_{p_2 \leftrightarrow p_4}, \end{aligned} \quad (59)$$

for $i = 1, 2, 3$. The denominators for this family of integrals can be respectively found by performing an exchange of p_2 and p_4 and $p_2 \rightarrow p_4$, $p_3 \rightarrow p_2$ and $p_4 \rightarrow p_3$ in the denominators presented in Table I.

$$\mathcal{H}_{e\mu,(- - ++)}^{(l)} = 2\mathcal{F}_{e\mu,1}^{(l)} - \mathcal{F}_{e\mu,2}^{(l)}. \quad (53)$$

We then multiply these expressions by their corresponding spinor structures.

$$\mathcal{A}_{e\mu,(\lambda_1 \lambda_2 \lambda_3 \lambda_4)}^{(l)} = \mathcal{H}_{e\mu,(\lambda_1 \lambda_2 \lambda_3 \lambda_4)}^{(l)} \Phi_{e\mu,(\lambda_1 \lambda_2 \lambda_3 \lambda_4)}. \quad (54)$$

One-Loop bare form factors

Here we present the one-loop bare form factors, $\mathcal{F}_{B;e\mu,i}^{(1)}$, in terms of integrals. These form factors can be directly obtained from $\mathcal{F}_{B;\mu\mu,i}^{(l)}$ as follows,

$$\mathcal{F}_{B;e\mu,1}^{(l)} = \mathcal{F}_{B;\mu\mu,1}^{(l)} \Big|_{p_2 \leftrightarrow p_4}, \quad (55)$$

$$\mathcal{F}_{B;e\mu,2}^{(l)} = \mathcal{F}_{B;\mu\mu,2}^{(l)} \Big|_{p_2 \leftrightarrow p_4}, \quad (56)$$

where the exchanging of p_2 and p_4 is understood as the exchange of s and t .

At one-loop, the form factors $F_{B;e\mu,i}^{(1)}$ become,

Two-loop bare form factors

Similarly to the one-loop case, to find the two-loop form factors for the $e^+\mu^- \rightarrow e^+\mu^-$ scattering, we can take the form factors from $e^+e^- \rightarrow \mu^+\mu^-$ then perform an exchange of s and t and exchange p_2 and p_4 in the integral families. However, at two-loop level this is more complicated. This is due to more families being present in the two-loop form factors of the $e^+e^- \rightarrow \mu^+\mu^-$ scattering. Therefore, we need to make sure we perform exchanges for all of the families.

For the planar families we have

$$d\log(\text{PL}1432, i) = d\log(\text{PL}1234, i) \Big|_{p_2 \leftrightarrow p_4}, \quad (60)$$

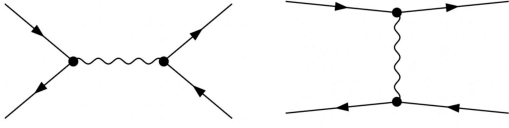


FIG. 5: The two tree-level diagrams that contribute to the $e^+e^- \rightarrow e^+e^-$ scattering. These diagrams were generated using FEYNARTS [44].

for $i = 1, 2, \dots, 8$.

Similarly, for the non-planar families we have:

$$d \log(\text{NPL1432}, i) = d \log(\text{NPL1234}, i) \Big|_{p_2 \leftrightarrow p_4}, \quad (61)$$

for $i = 1, 2, \dots, 12$.

Similar exchanges must be performed for all families that appear in the form factors of the $e^+e^- \rightarrow \mu^+\mu^-$ scattering. The families that appear are listed in Appendix B.

The explicit expressions for the two-loop bare form factors can be found in the ancillary files.

C. $e^+e^- \rightarrow e^+e^-$

Similarly to the previous process, the $e^+e^- \rightarrow e^+e^-$ process can be derived from the helicity amplitudes of the $e^+e^- \rightarrow \mu^+\mu^-$ and $e^+\mu^- \rightarrow e^+\mu^-$.

As all fermions are of the same flavour, additional fermionic currents are possible. Meaning that both the diagrams from the $e^+e^- \rightarrow e^+e^-$ scattering and those from the $e^+e^- \rightarrow \mu^+\mu^-$ and $e^+\mu^- \rightarrow e^+\mu^-$ contribute to the scattering amplitude. This can be seen in Fig. 5.

We obtained the form factors for the $e^+\mu^- \rightarrow e^+\mu^-$ scattering via an exchange of the particles with momenta p_2 and p_4 . However, for $e^+e^- \rightarrow e^+e^-$ if we consider the same exchange, identical fermions will be exchanged. Therefore, we must include a change of sign for all of the diagrams that can be obtained by this exchange. We are then able to combine the form factors that come from all diagrams to obtain the helicity amplitudes.

As with the $e^+e^- \rightarrow \mu^+\mu^-$ scattering, there are only 4 non-vanishing helicities. Therefore, we can present the tensor structures in the form of Eq. (42). To obtain the helicity amplitudes for the $e^+e^- \rightarrow e^+e^-$ scattering, we use the following combinations of the form factors.

$$\begin{aligned} \mathcal{H}_{ee,(-+++)}^{(l)} &= -2\mathcal{F}_{\mu\mu,1}^{(l)} + (1-x)\mathcal{F}_{\mu\mu,2}^{(l)}, \\ \mathcal{H}_{ee,(-++-)}^{(l)} &= -2\mathcal{F}_{\mu\mu,1}^{(l)} - x\mathcal{F}_{\mu\mu,2}^{(l)} - 2\mathcal{F}_{e\mu,1}^{(l)} + \mathcal{F}_{e\mu,2}^{(l)}. \end{aligned} \quad (62)$$

Note that in the $(-++-)$ configuration the crossed diagrams don't contribute. This is as helicity conservation is not possible for the $e^+\mu^- \rightarrow e^+\mu^-$ scattering in this helicity configuration.

From here we can obtain the following helicity amplitudes:

$$\mathcal{A}_{ee,(\lambda_1\lambda_2\lambda_3\lambda_4)}^{(l)} = \mathcal{H}_{ee,(\lambda_1\lambda_2\lambda_3\lambda_4)}^{(l)} \Phi_{\mu\mu,(\lambda_1\lambda_2\lambda_3\lambda_4)}. \quad (63)$$

D. $e^+e^- \rightarrow \gamma\gamma$

For the $e^+e^- \rightarrow \gamma\gamma$ scattering there are 4 independent Lorentz structures that can appear in the amplitudes of contributing Feynman diagrams.

$$\begin{aligned} T_{\gamma\gamma,1} &= \bar{u}(p_2)\not{\varepsilon}_3u(p_1)(p_2 \cdot \varepsilon_4), \\ T_{\gamma\gamma,2} &= \bar{u}(p_2)\not{\varepsilon}_4u(p_1)(p_1 \cdot \varepsilon_3), \\ T_{\gamma\gamma,3} &= \bar{u}(p_2)\not{p}_3u(p_1)(p_1 \cdot \varepsilon_3)(p_2 \cdot \varepsilon_4), \\ T_{\gamma\gamma,4} &= \bar{u}(p_2)\not{p}_3u(p_1)(\varepsilon_3 \cdot \varepsilon_4), \end{aligned} \quad (64)$$

where ε_i represent the polarisation vectors of the photons with momenta p_3 and p_4 . These polarisation vectors can be written in the spinor-helicity formalism as,

$$\begin{aligned} \varepsilon_{3,-}^\mu &= \frac{\langle 3|\gamma^\mu|2\rangle}{\sqrt{2}\langle 32\rangle}, & \varepsilon_{3,+}^\mu &= \frac{\langle 2|\gamma^\mu|3\rangle}{\sqrt{2}\langle 23\rangle}, \\ \varepsilon_{4,-}^\mu &= \frac{\langle 4|\gamma^\mu|1\rangle}{\sqrt{2}\langle 41\rangle}, & \varepsilon_{4,+}^\mu &= \frac{\langle 1|\gamma^\mu|4\rangle}{\sqrt{2}\langle 14\rangle}. \end{aligned} \quad (65)$$

Here we have set p_2 as a reference momentum for ε_3 and p_1 as a reference momentum for ε_4 , such that $\varepsilon_3 \cdot p_2 = \varepsilon_4 \cdot p_1 = 0$.

The tensor structures in Eq. (64) define the 4 form factors that we compute in our calculation of helicity amplitudes.

For these tensor structures there are 8 non-vanishing helicity configurations that can be seen below,

$$\begin{aligned} \{ & -+-- , -+++ , -+-+ , -+ +- , \\ & +-++ , +--- , +-+- , +--+ \}. \end{aligned} \quad (66)$$

In a similar way to the $e^+e^- \rightarrow \mu^+\mu^-$ process, we will present the first four helicities in our results. The other helicity configurations can be obtained by applying parity transformations.

The spinor helicity representation that we will use for the first four helicities respectively are:

$$\begin{aligned} & \{ \Phi_{\gamma\gamma,(-+--)}, \Phi_{\gamma\gamma,(-+++)}, \Phi_{\gamma\gamma,(-+-+)}, \Phi_{\gamma\gamma,(-+ +-)} \} \\ & = \left\{ \frac{\langle 14\rangle [24] \langle 34\rangle \langle 14\rangle [24] [34]}{[34]}, \frac{\langle 13\rangle [14] [24] \langle 14\rangle \langle 24\rangle [23]}{[13]}, \frac{\langle 14\rangle [24] [34]}{\langle 34\rangle}, \frac{\langle 13\rangle [14] [24] \langle 14\rangle \langle 24\rangle [23]}{\langle 23\rangle} \right\}. \end{aligned} \quad (67)$$

As with the $e^+e^- \rightarrow \mu^+\mu^-$ scattering we also have to consider pre-factors to each of the form factors when constructing the helicity amplitudes. The sums we require are:

$$\mathcal{H}_{\gamma\gamma,(-+--)}^{(l)} = -\frac{1}{x}\mathcal{F}_{\gamma\gamma,2}^{(l)} - \frac{(1-x)}{2x}\mathcal{F}_{\gamma\gamma,3}^{(l)} - \frac{1}{x}\mathcal{F}_{\gamma\gamma,4}^{(l)},$$

$$\begin{aligned}
\mathcal{H}_{\gamma\gamma,(-++++)}^{(l)} &= \frac{1}{x}\mathcal{F}_{\gamma\gamma,1}^{(l)} - \frac{(1-x)}{2x}\mathcal{F}_{\gamma\gamma,3}^{(l)} - \frac{1}{x}\mathcal{F}_{\gamma\gamma,4}^{(l)}, \\
\mathcal{H}_{\gamma\gamma,(-++-)}^{(l)} &= \frac{(1-x)}{2x}\mathcal{F}_{\gamma\gamma,3}^{(l)} + \frac{(1-x)}{x}\mathcal{F}_{\gamma\gamma,4}^{(l)}, \\
\mathcal{H}_{\gamma\gamma,(-+-+)}^{(l)} &= -\frac{1}{x}\mathcal{F}_{\gamma\gamma,1}^{(l)} + \frac{1}{x}\mathcal{F}_{\gamma\gamma,2}^{(l)} \\
&\quad + \frac{(1-x)}{2x}\mathcal{F}_{\gamma\gamma,3}^{(l)} + \frac{(1-x)}{x}\mathcal{F}_{\gamma\gamma,4}^{(l)}. \quad (68)
\end{aligned}$$

We then multiply these expressions by their corresponding spinor structures,

$$\mathcal{A}_{\gamma\gamma,(\lambda_1\lambda_2\lambda_3\lambda_4)}^{(l)} = \mathcal{H}_{\gamma\gamma,(\lambda_1\lambda_2\lambda_3\lambda_4)}^{(l)} \Phi_{\gamma\gamma,(\lambda_1\lambda_2\lambda_3\lambda_4)}. \quad (69)$$

From the relations discussed in this section, we obtain helicity amplitudes for all processes at tree level, one loop, and two loops. In the following section, we proceed to verify these results.

V. CHECKS

For all the processes we have considered we have obtained expressions that are free from ϵ poles. This is already a very good indicator that our results are accurate. However, we must also confirm that higher orders in the dimensional regulator in our expressions are also valid.

To ensure that our results are consistent at higher orders in the dimensional regulator we performed checks against existing results up to the same ϵ order in corresponding QCD processes. Namely, we can compare:

- $e^+e^- \rightarrow \mu^+\mu^-$ with $q\bar{q} \rightarrow Q\bar{Q}$ [8, 9],
- $e^+\mu^- \rightarrow e^+\mu^-$ with $q\bar{Q} \rightarrow q\bar{Q}$ [9],
- $e^+e^- \rightarrow e^+e^-$ with $q\bar{q} \rightarrow q\bar{q}$ [9],
- $e^+e^- \rightarrow \gamma\gamma$ with $q\bar{q} \rightarrow gg$ [8, 10].

Whilst this is an incredibly beneficial check, we cannot make an immediate direct comparison because the QCD processes involve additional contributing diagrams which are non-Abelian. There is an extra level of intricacy as we also have to consider the colour structure of quarks and gluons in QCD. Therefore, we need to identify the contributions to the QCD scattering amplitudes that correspond solely to the Abelian diagrams present in QED.

We will discuss each process separately as they require slightly different treatments.

A. Notation

Throughout this section, we set our notation to present the checks on our results in a concise way. Firstly, we will represent the helicity amplitudes in form of

Eqs. (38) and (39). $A_p^{(l)}, B_p^{(l)}, C_p^{(l)}$ represent combinations of Abelian diagrams at l loops and p denotes the process we are considering. Additionally, to extract the relevant pieces of the QCD amplitude,⁸ we employ the notation,

$$\langle \mathcal{M}_X^{(l)} | \mathcal{C}_j \rangle_{[k,m]}. \quad (70)$$

The indices in this notation can be understood as:

- X is the QCD process,
- l is the loop order,
- j informs us which colour structure is being considered,
- k tells us which power of N_c we are considering, with N_c representing the number of colours.
- m tells us which power of N_f we are considering.

It is also worth noting that, in order to make our checks, we must make an exchange of $x \rightarrow 1-x$ as in our calculation the external particles p_3 and p_4 are swapped compared to [8–10] against which we will be completing our checks.

Additionally, in order to establish consistency between the results, we must ensure that the spinor helicity structures that appear are equivalent. Therefore, we added a helicity dependent kinematic pre-factor to each of the helicity amplitudes provided in [8–10].

As [8] provides the bare helicity amplitudes, when comparing our results we must compare helicity amplitudes from our bare form factors rather than our final helicity amplitudes with poles removed. Due to a subtlety in the dimensional regularisation, a comparison order-by-order in ϵ between $e^+e^- \rightarrow \mu^+\mu^-$ and $q\bar{q} \rightarrow Q\bar{Q}$ in [8] is not straightforward. This is as the tensor structures used in the decomposition of the amplitudes have explicit dependence on the dimensional regulator ϵ . This means that whilst the finite remainder after UV renormalisation and IR subtraction would agree, bare helicity amplitudes do not. The same issue was reported in [9] as the authors of this reference performed similar cross-checks.

The bare helicity amplitudes for $q\bar{q} \rightarrow gg$ are also provided in [8], therefore we are able to compare our helicity amplitudes of $e^+e^- \rightarrow \gamma\gamma$ from our bare form factors with the helicity amplitudes presented in [8]. The same subtlety in the dimensional regularisation does not appear to affect the results of this process. In the decomposition of $q\bar{q} \rightarrow gg$, Ref. [8] uses 5 alternative tensors structures as opposed to the 4 tensor structures that we use. However, we were able to find full agreement for the bare helicity amplitudes at tree-level, one- and two-loop at all orders in ϵ that are presented.

⁸ A similar organisation of Feynman diagrams present in the scattering of four fermions in QED and in QCD has been carried out in [54].

B. Checks on $e^+e^- \rightarrow \mu^+\mu^-$

To perform our checks for the $e^+e^- \rightarrow \mu^+\mu^-$ scattering amplitude we make a comparison against the results obtained in [9]. The colour structures we have to consider for this process are:

$$\begin{aligned} \mathcal{C}_1 &= \delta_{i_1 i_3} \delta_{i_2 i_4}, \\ \mathcal{C}_2 &= \delta_{i_1 i_2} \delta_{i_3 i_4}, \end{aligned} \quad (71)$$

where δ_{ij} is the colour delta function.

The helicity amplitudes for this process take the form of Eq. (38). To verify our results, we make comparisons between QED and QCD using the following relations:

- Tree-Level

$$A_{\mu\mu}^{(0)} = -2 \times \langle \mathcal{M}_{Q\bar{Q}}^{(0)} | \mathcal{C}_2 \rangle_{[-1,0]}. \quad (72)$$

- One-Loop

$$A_{\mu\mu}^{(1)} = 2 \times \langle \mathcal{M}_{Q\bar{Q}}^{(1)} | \mathcal{C}_2 \rangle_{[-2,0]}, \quad (73a)$$

$$B_{\mu\mu}^{(1)} = -2 \times \langle \mathcal{M}_{Q\bar{Q}}^{(1)} | \mathcal{C}_2 \rangle_{[-1,1]}. \quad (73b)$$

- Two-Loop

$$A_{\mu\mu}^{(2)} = -2 \times \langle \mathcal{M}_{Q\bar{Q}}^{(2)} | \mathcal{C}_2 \rangle_{[-3,0]}, \quad (74a)$$

$$B_{\mu\mu}^{(2)} = 2 \times \langle \mathcal{M}_{Q\bar{Q}}^{(2)} | \mathcal{C}_2 \rangle_{[-2,1]}, \quad (74b)$$

$$C_{\mu\mu}^{(2)} = -2 \times \langle \mathcal{M}_{Q\bar{Q}}^{(2)} | \mathcal{C}_2 \rangle_{[-1,2]}. \quad (74c)$$

Using these comparisons, we find complete agreement with the QCD results in [9] at all orders in ϵ at one and two loops.

C. Checks on $e^+\mu^- \rightarrow e^+\mu^-$

To perform our checks for the $e^+\mu^- \rightarrow e^+\mu^-$ scattering amplitude, we make a comparison against the results obtained in [9]. Here, the colour structures we have to consider for this process are:

$$\begin{aligned} \mathcal{C}_1 &= \delta_{i_1 i_4} \delta_{i_2 i_3}, \\ \mathcal{C}_2 &= \delta_{i_1 i_2} \delta_{i_3 i_4}. \end{aligned} \quad (75)$$

Similar to $e^+e^- \rightarrow \mu^+\mu^-$, we make the following comparisons:

- Tree-Level

$$A_{e\mu}^{(0)} = -2 \times \langle \mathcal{M}_{q\bar{Q}}^{(0)} | \mathcal{C}_1 \rangle_{[-1,0]}. \quad (76)$$

- One-Loop

$$A_{e\mu}^{(1)} = 2 \times \langle \mathcal{M}_{q\bar{Q}}^{(1)} | \mathcal{C}_1 \rangle_{[-2,0]}, \quad (77a)$$

$$B_{e\mu}^{(1)} = -2 \times \langle \mathcal{M}_{q\bar{Q}}^{(1)} | \mathcal{C}_1 \rangle_{[-1,1]}. \quad (77b)$$

- Two-Loop

$$A_{e\mu}^{(2)} = -2 \times \langle \mathcal{M}_{q\bar{Q}}^{(2)} | \mathcal{C}_1 \rangle_{[-3,0]}, \quad (78a)$$

$$B_{e\mu}^{(2)} = 2 \times \langle \mathcal{M}_{q\bar{Q}}^{(2)} | \mathcal{C}_1 \rangle_{[-2,1]}, \quad (78b)$$

$$C_{e\mu}^{(2)} = -2 \times \langle \mathcal{M}_{q\bar{Q}}^{(2)} | \mathcal{C}_1 \rangle_{[-1,2]}. \quad (78c)$$

Using these comparisons, we find complete agreement with the QCD results in [9] at one and two loops.

D. Checks on $e^+e^- \rightarrow e^+e^-$

To perform our checks for the $e^+e^- \rightarrow e^+e^-$ scattering amplitude, we make a comparison against the results obtained for the same flavour process in [9]. The colour structures we have to consider for this process are also the same as those considered in Eq. (75). The helicity amplitudes for this process also take the form of Eq. (38). However, our checks are slightly different as both colour structures need to be considered, as seen below:

- Tree-Level

$$A_{ee}^{(0)} = -2 \times \left(\langle \mathcal{M}_{q\bar{q}}^{(0)} | \mathcal{C}_1 \rangle_{[-1,0]} + \langle \mathcal{M}_{q\bar{q}}^{(0)} | \mathcal{C}_2 \rangle_{[-1,0]} \right). \quad (79)$$

- One-Loop

$$A_{ee}^{(1)} = 2 \times \left(\langle \mathcal{M}_{q\bar{q}}^{(1)} | \mathcal{C}_1 \rangle_{[-2,0]} + \langle \mathcal{M}_{q\bar{q}}^{(1)} | \mathcal{C}_2 \rangle_{[-2,0]} \right), \quad (80a)$$

$$B_{ee}^{(1)} = -2 \times \left(\langle \mathcal{M}_{q\bar{q}}^{(1)} | \mathcal{C}_1 \rangle_{[-1,1]} + \langle \mathcal{M}_{q\bar{q}}^{(1)} | \mathcal{C}_2 \rangle_{[-1,1]} \right). \quad (80b)$$

- Two-Loop

$$A_{ee}^{(2)} = -2 \times \left(\langle \mathcal{M}_{q\bar{q}}^{(2)} | \mathcal{C}_1 \rangle_{[-3,0]} + \langle \mathcal{M}_{q\bar{q}}^{(2)} | \mathcal{C}_2 \rangle_{[-3,0]} \right), \quad (81a)$$

$$B_{ee}^{(2)} = 2 \times \left(\langle \mathcal{M}_{q\bar{q}}^{(2)} | \mathcal{C}_1 \rangle_{[-2,1]} + \langle \mathcal{M}_{q\bar{q}}^{(2)} | \mathcal{C}_2 \rangle_{[-2,1]} \right), \quad (81b)$$

$$C_{ee}^{(2)} = -2 \times \left(\langle \mathcal{M}_{q\bar{q}}^{(2)} | \mathcal{C}_1 \rangle_{[-1,2]} + \langle \mathcal{M}_{q\bar{q}}^{(2)} | \mathcal{C}_2 \rangle_{[-1,2]} \right). \quad (81c)$$

Using these comparisons, we find complete agreement with the QCD results in QCD results in [9] at all orders in ϵ at one and two loops.

E. Checks on $e^+e^- \rightarrow \gamma\gamma$

To perform our checks for the $e^+e^- \rightarrow \gamma\gamma$ scattering amplitude we make a comparison against the results obtained in [8, 10]. The colour structures we have to consider for this process are:

$$\begin{aligned}\mathcal{C}_1 &= (T^{a_3}T^{a_4})_{i_2i_1}, \\ \mathcal{C}_2 &= (T^{a_4}T^{a_3})_{i_2i_1}, \\ \mathcal{C}_3 &= \delta^{a_3a_4}\delta_{i_2i_1}.\end{aligned}\quad (82)$$

Complications arise when making comparisons in this process, particularly when comparing the terms proportional to N_f . This is as we need to consider linear combinations of pieces of the QCD amplitude that correspond to different colour structures and, in some cases, orders of N_c also. We have to consider these combinations to ensure that all of the Abelian diagrams are included and that each diagram only contributes once.

In order to verify our results for the helicity amplitudes of this process, we cross-checked against QCD results in the following way:

- Tree-Level

$$A_{\gamma\gamma}^{(0)} = 2 \times \left(\langle \mathcal{M}_{gg}^{(0)} | \mathcal{C}_1 \rangle_{[0,0]} + \langle \mathcal{M}_{gg}^{(0)} | \mathcal{C}_2 \rangle_{[0,0]} \right). \quad (83)$$

- One-Loop

$$A_{\gamma\gamma}^{(1)} = -2 \times \left(\langle \mathcal{M}_{gg}^{(1)} | \mathcal{C}_1 \rangle_{[-1,0]} + \langle \mathcal{M}_{gg}^{(1)} | \mathcal{C}_2 \rangle_{[-1,0]} \right). \quad (84)$$

- Two-Loop

$$A_{\gamma\gamma}^{(2)} = 2 \times \left(\langle \mathcal{M}_{gg}^{(2)} | \mathcal{C}_1 \rangle_{[-2,0]} + \langle \mathcal{M}_{gg}^{(2)} | \mathcal{C}_2 \rangle_{[-2,0]} \right), \quad (85a)$$

$$\begin{aligned}B_{\gamma\gamma}^{(2)} &= -2 \times \left(\langle \mathcal{M}_{gg}^{(2)} | \mathcal{C}_1 \rangle_{[-1,1]} + \langle \mathcal{M}_{gg}^{(2)} | \mathcal{C}_2 \rangle_{[-1,1]} \right. \\ &\quad \left. + 2 \times \langle \mathcal{M}_{gg}^{(2)} | \mathcal{C}_3 \rangle_{[-2,1]} \right). \quad (85b)\end{aligned}$$

Note that for the case of $B_{\gamma\gamma}^{(2)}$, we have to use a linear combination of the colours with differing coefficients. We use this linear combination to ensure that we only extract one contribution from each Abelian diagram from the QCD amplitude.

Using these comparisons, we find complete agreement with the QCD results in [10] at all orders in ϵ at one and two loops. Additionally, using the same comparisons on bare helicity amplitudes provided in [8], we were able to find agreement at all orders in ϵ at one and two loops as well.

F. Iterative IR structure of the amplitudes

In this section, we aim to clarify the differences between the results for $q\bar{q} \rightarrow Q\bar{Q}$, as presented in [8], and the process $e^+e^- \rightarrow \mu^+\mu^-$ computed in this paper.

From relations (43), we express our helicity amplitudes in terms of master integrals admitting a d log representation. By inspecting the expression of these amplitudes, we identify a drop in the maximal transcendental degree in terms proportional to N_f and N_f^2 . In detail, we observe that,

$$\mathcal{H}_{\mu\mu(\lambda_1\lambda_2\lambda_3\lambda_4)}^{(2)} \sim \tilde{A}_{\mu\mu}^{(2)} + \epsilon N_f \tilde{B}_{\mu\mu}^{(2)} + \epsilon^2 N_f^2 \tilde{C}_{\mu\mu}^{(2)}. \quad (86)$$

After performing UV renormalisation on our expressions, following (27), and comparing with the results in [8] once their expressions are renormalised, we find complete agreement in terms proportional to N_f^2 . For terms proportional to N_f and N_f^0 , we observe agreement up to the ϵ^{-1} and ϵ^{-2} poles, respectively. At higher orders in ϵ , both results exhibit the same functional structure when considering the maximal transcendental weight. This indicates to differences in regularisation schemes, as mentioned above.

To address this discrepancy, we can examine the iterative IR structure of the amplitude by taking the logarithm of our renormalised amplitudes,

$$\begin{aligned}\log \mathcal{M}_{\lambda_1\lambda_2\lambda_3\lambda_4} &= \left(\frac{\alpha}{2\pi} \right) \left[\mathcal{M}_{\lambda_1\lambda_2\lambda_3\lambda_4}^{(1)} \right. \\ &\quad \left. + \left(\frac{\alpha}{2\pi} \right) \left(\mathcal{M}_{\lambda_1\lambda_2\lambda_3\lambda_4}^{(2)} - \frac{1}{2} \left(\mathcal{M}_{\lambda_1\lambda_2\lambda_3\lambda_4}^{(1)} \right)^2 \right) \right] + \mathcal{O}(\alpha^3),\end{aligned}\quad (87)$$

with,

$$\mathcal{M}_{\lambda_1\lambda_2\lambda_3\lambda_4}^{(l)} = \frac{A_{\lambda_1\lambda_2\lambda_3\lambda_4}^{(l)}}{A_{\lambda_1\lambda_2\lambda_3\lambda_4}^{(0)}}. \quad (88)$$

By focusing on the α^2 contribution, we obtain for the four-fermion scattering in both QED and QCD (considering only the sum of Abelian diagrams),

$$\begin{aligned}\mathcal{M}_{\mu\mu(\lambda_1\lambda_2\lambda_3\lambda_4)}^{(2)} &- \frac{1}{2} \left(\mathcal{M}_{\mu\mu(\lambda_1\lambda_2\lambda_3\lambda_4)}^{(1)} \right)^2 \\ &= -\frac{1}{\epsilon^3} N_f \\ &\quad + \frac{2}{3\epsilon^2} N_f \left[-\frac{2}{3} + (L_{34} + L_{23} - L_{24}) \right] \\ &\quad + \frac{1}{\epsilon} \left[\gamma_1^q + \frac{\gamma_1^{\text{cusp}}}{2} (L_{34} + L_{23} - L_{24}) \right] \\ &\quad + E_{\mu\mu(\lambda_1\lambda_2\lambda_3\lambda_4)} + \mathcal{O}(\epsilon).\end{aligned}\quad (89)$$

This result confirms that these scheme-dependent differences are resolved for four-fermion scattering processes in the chosen framework.

The very similar behaviour is observed for the scattering processes $q\bar{q} \rightarrow gg$ and $e^+e^- \rightarrow \gamma\gamma$,

$$\begin{aligned}\mathcal{M}_{\gamma\gamma(\lambda_1\lambda_2\lambda_3\lambda_4)}^{(2)} &- \frac{1}{2} \left(\mathcal{M}_{\gamma\gamma(\lambda_1\lambda_2\lambda_3\lambda_4)}^{(1)} \right)^2 \\ &= -\frac{1}{2\epsilon^3} N_f\end{aligned}\quad (90)$$

$$\begin{aligned}
& + \frac{1}{3\epsilon^2} N_f \left[\frac{2}{3} N_f + \left(-\frac{2}{3} + L_{34} \right) \right] \\
& + \frac{1}{2\epsilon} \left[\gamma_1^g + \gamma_1^q + \frac{\gamma_1^{\text{cusp}}}{2} L_{34} \right] \\
& + E_{\gamma\gamma(\lambda_1\lambda_2\lambda_3\lambda_4)} + \mathcal{O}(\epsilon) ,
\end{aligned}$$

In Eqs. (89) and (90), E contains information on the finite remainder, which depends on the helicity configuration.

The observation that we find the same iterative IR structure in both our results and the Abelian contributions from the results presented in [8], is confirmation that the discrepancies in our results stem only from the difference in regularisation schemes.

VI. DISCUSSION AND OUTLOOK

In this paper, we analytically calculated one- and two-loop helicity amplitudes for the massless QED scattering processes:

$$\begin{aligned}
e^+ e^- & \rightarrow \mu^+ \mu^- , \\
e^+ \mu^- & \rightarrow e^+ \mu^- , \\
e^+ e^- & \rightarrow e^+ e^- , \\
e^+ e^- & \rightarrow \gamma\gamma ,
\end{aligned}$$

at higher orders in the dimensional regulator ϵ , by decomposing these physical amplitudes in terms of four-dimensional form factors. We performed this decomposition by profiting from the dimensionality of the external momenta and closely adopted the 't Hooft-Veltman regularisation scheme. Our results for non-vanishing helicity amplitudes, after performing UV renormalisation and IR subtraction, are expressed in terms of generalised polylogarithms up to transcendental weight six.

In addition to the standard approach to calculate multi-loop scattering amplitudes, we proposed an algorithm at integrand level, based on matrix transformations, to organise multi-loop Feynman diagrams into families. We motivated this method to simplify the complexity in the solution of IBP systems, by allowing us to identify a minimal set of master integrals that we chose them to admit a $d \log$ representation.

We observed that, by carefully extracting Abelian contributions from the QCD counterpart processes, we were able to verify our QED results.

With the explicit evaluation of these scattering amplitudes, there are several directions. The techniques we have employed are directly applicable to the calculation of three-loop scattering amplitudes, which will complete the necessary ingredients for theoretical predictions at N³LO. Additionally, we expect that our algorithm for grouping Feynman diagrams will be applicable for other physical processes involving internal massive particles. Furthermore, we foresee the four-dimensional tensor decomposition to facilitate efficient calculations of physical processes of interest at low energies.

ACKNOWLEDGEMENTS

We thank Giulio Gambuti and Lorenzo Tancredi for sharing updated results of Ref. [9] with us. We also wish to thank Giulio Crisanti, Manoj Mandal, Pierpaolo Mastrolia, Jonathan Ronca and Sid Smith for collaboration on closely related projects, and Taushif Ahmed and Einar Gardi for useful discussions. This work is supported by the Leverhulme Trust, LIP-2021-01. We acknowledge the Mainz Institute for Theoretical Physics (MITP) of the Cluster of Excellence PRISMA⁺ (Project ID 390831469), for its hospitality.

Appendix A: Results obtained via Matrix-Based Method

Utilising the algorithm presented in Sec. II C for the $e^+e^- \rightarrow \mu^+\mu^-$ process, we find shifts for all diagrams apart from 2 (for which there was no possible shift of loop momenta). These 2 diagrams were then defined as additional parent diagrams, giving 18 families altogether. Table III shows how many diagrams, including the parent topology, appear in each family.

Analogously, for the $e^+e^- \rightarrow \gamma\gamma$ process, we find that there were shifts for all diagrams into 20 families. Table IV shows matching information for this process.

Parent Diagram	# Diagrams	
Planar	Diagram 16	5
	Diagram 19	2
	Diagram 20	30
	Diagram 22	5
	Diagram 23	2
	Diagram 25	6
	Diagram 26	4
	Diagram 27	4
	Diagram 28	2
	Diagram 29	1
	Diagram 31	1
	Diagram 32	1
	Non-Planar	Diagram 17
Diagram 18		1
Diagram 30		1
Diagram 33		1
Diagram 49		1

TABLE III: Families for $e^+e^- \rightarrow \mu^+\mu^-$.

Parent Diagram	# Diagrams	
Planar	Diagram 49	9
	Diagram 52	6
	Diagram 53	25
	Diagram 58	10
	Diagram 63	5
	Diagram 68	14
	Diagram 69	7
	Diagram 70	7
	Diagram 71	2
	Diagram 73	8
	Diagram 74	9
	Diagram 78	2
	Diagram 80	9
	Diagram 84	8
Non-Planar	Diagram 47	6
	Diagram 50	4
	Diagram 51	7
	Diagram 59	4
	Diagram 79	3

TABLE IV: Families for $e^+e^- \rightarrow \gamma\gamma$.

The Feynman diagrams for the parent topologies that define each family can be found in Figs. 6 and 7. These tables summarise information about the families that the integrands are grouped into (see Sec. II E for the definition of the families).

Appendix B: Canonical integral families

Canonical families for $e^+e^- \rightarrow \mu^+\mu^-$

For the one-loop case, the integrals that appear in families 1234 and 1243 provide a sufficient basis of MIs to express all scalar integrals that appear.

At two-loop, we are able to express all integrals in terms of 7 integral families. As mentioned in Sec. II E, we prioritise planar integrals over non-planar integrals. This allows us to reduce from the 120 canonical integrals (from 12 families) to just 35 MIs that stem from 7 families.

Namely, we can reduce our form factors to integrals appearing in the planar families: PL1234, PL1243, PL1342, PL1432, and in the non-planar families: NPL1234, NPL1243, NPL1432.

Canonical families for $e^+e^- \rightarrow \gamma\gamma$

As with the $e^+e^- \rightarrow \mu^+\mu^-$ process in the one-loop case, the integral families 1234 and 1243 provide a sufficient basis of MIs to express all scalar integrals that appear.

For the two-loop case of this process, we are able to express all integrals in terms of 39 MIs that originate from 9 integral families. These families are comprised of all of the 6 planar families and 3 non-planar families.

The planar families are: PL1234, PL1243, PL1324, PL1342, PL1423, PL1432, as well as the non-planar families: NPL1234, NPL1243, NPL1342.

The denominators for the families required for each process can be obtained using the propagators in Table II and performing any necessary exchanges of momenta.

The definitions of these integrals in terms of scalar in-

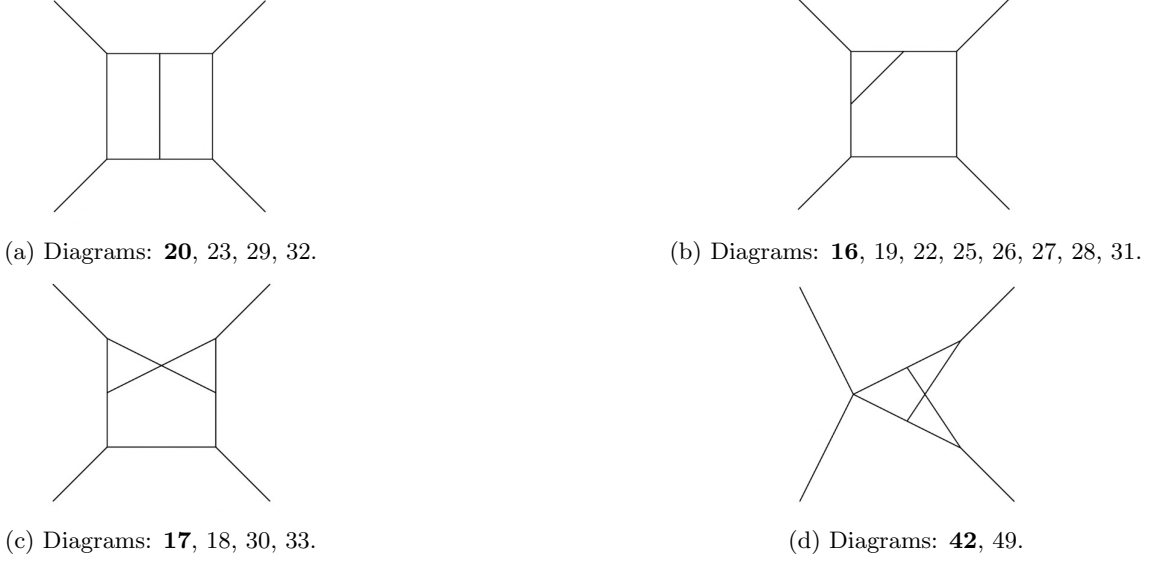


FIG. 6: Parent topologies present in the two-loop scattering amplitude $e^+e^- \rightarrow \mu^+\mu^-$. Here and in Fig. 7, the numbers in bold are the diagrams represented by the Figure in the standard momenta ordering, the others can be found via exchanges of external momenta.

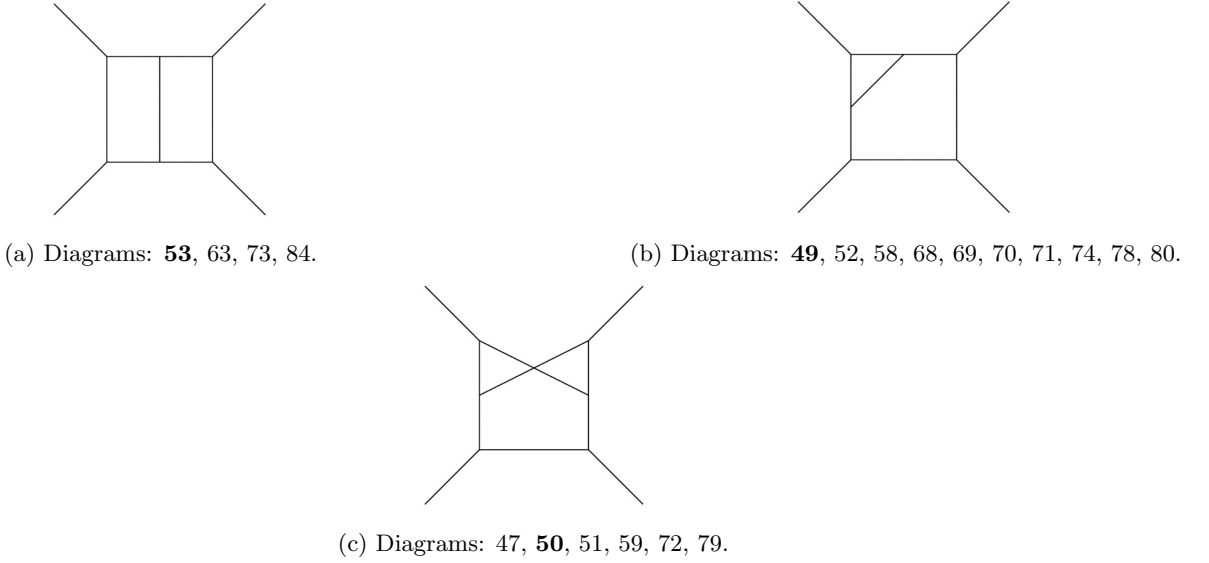


FIG. 7: Parent topologies present in the two-loop $e^+e^- \rightarrow \gamma\gamma$.

tegrals can be found within the ancillary files.

and

Appendix C: Details on IR subtraction

For $e^+e^- \rightarrow \mu^+\mu^-$ and $e^+e^- \rightarrow \gamma\gamma$, we can, respectively, use the following formulae for the elements of the anomalous dimension matrix Γ :

$$\Gamma_{\mu\mu; n} = -2\gamma_n^{\text{cusp}} (L_{34} + L_{23} - L_{24}) + 4\gamma_n^q, \quad (\text{C1})$$

$$\Gamma_{\gamma\gamma; n} = -\gamma_n^{\text{cusp}} (L_{34}) + 2\gamma_n^q + 2\gamma_n^g, \quad (\text{C2})$$

$$\Gamma'_{\mu\mu; n} = \frac{\partial \Gamma_{\mu\mu; n}}{\partial \log(\mu)} = -4\gamma_n^{\text{cusp}}, \quad (\text{C3})$$

$$\Gamma'_{\gamma\gamma; n} = \frac{\partial \Gamma_{\gamma\gamma; n}}{\partial \log(\mu)} = -2\gamma_n^{\text{cusp}}. \quad (\text{C4})$$

Below, we list the anomalous dimension coefficients for the relevant particles in our processes. We obtained these values considering the coefficients of $\left(\frac{\alpha_s^{(n_1)}}{2\pi}\right)^{n+1}$ in the expansions given in [55–58], once we abelianised

these expansions by setting $C_A \rightarrow 0$, $C_F \rightarrow 1$, and $T_F \rightarrow 1$.

The cusp anomalous dimension

$$\begin{aligned}\gamma_0^{\text{cusp}} &= 2, \\ \gamma_1^{\text{cusp}} &= -\frac{20}{9}N_f.\end{aligned}\tag{C5}$$

The quark anomalous dimension

$$\begin{aligned}\gamma_0^q &= -\frac{3}{2}, \\ \gamma_1^q &= \left(\frac{65}{54} + \frac{\pi^2}{6}\right)N_f + \left(\frac{\pi^2}{2} - 6\zeta_3 - \frac{3}{8}\right).\end{aligned}\tag{C6}$$

The gluon anomalous dimension

$$\begin{aligned}\gamma_0^g &= -\beta_0, \\ \gamma_1^g &= -\beta_1.\end{aligned}\tag{C7}$$

Appendix D: Organisation of the ancillary files

In this appendix we outline the organisation of the ancillary files included on the arXiv submission of this paper:

- **Bare_FF**s/: we provide the decompositions of the bare form factors for the processes $e^+e^- \rightarrow \mu^+\mu^-$, $e^+\mu^- \rightarrow e^+\mu^-$ and $e^+e^- \rightarrow \gamma\gamma$ at tree level, one-loop, and two-loop level in terms of master integrals. We also provide additional files where we express these master integrals in terms of GPLs.
- **Results**/: in this folder we include the decompositions of the UV renormalised and IR subtracted form factors, which are free from poles, for each process at each loop order.
- **Helicity_Amplitudes**/: we supply the non-vanishing helicity amplitudes, that are free from poles, for all processes across tree level, one-loop and two-loop orders.
- **Families**/: we provide the master integrals in the form of scalar integrals (15), for all families. The denominators of these scalar integrals can be deduced from Tables I and II.

-
- [1] G. Heinrich, *Collider Physics at the Precision Frontier*, *Phys. Rept.* **922** (2021) 1–69, [2009.00516].
- [2] J. Huston, K. Rabbertz and G. Zanderighi, *Quantum Chromodynamics*, **2312.14015**.
- [3] J. Andersen et al., *Les Houches 2023: Physics at TeV Colliders: Standard Model Working Group Report*, in *Physics of the TeV Scale and Beyond the Standard Model: Intensifying the Quest for New Physics*, 6, 2024. **2406.00708**.
- [4] C. Anastasiou, E. W. N. Glover, C. Oleari and M. E. Tejeda-Yeomans, *Two-loop QCD corrections to the scattering of massless distinct quarks*, *Nucl. Phys. B* **601** (2001) 318–340, [hep-ph/0010212].
- [5] C. Anastasiou, E. W. N. Glover, C. Oleari and M. E. Tejeda-Yeomans, *Two loop QCD corrections to massless identical quark scattering*, *Nucl. Phys. B* **601** (2001) 341–360, [hep-ph/0011094].
- [6] C. Anastasiou, E. W. N. Glover, C. Oleari and M. E. Tejeda-Yeomans, *Two loop QCD corrections to massless quark gluon scattering*, *Nucl. Phys. B* **605** (2001) 486–516, [hep-ph/0101304].
- [7] C. Anastasiou, E. W. N. Glover and M. E. Tejeda-Yeomans, *Two loop QED and QCD corrections to massless fermion boson scattering*, *Nucl. Phys. B* **629** (2002) 255–289, [hep-ph/0201274].
- [8] T. Ahmed, J. Henn and B. Mistlberger, *Four-particle scattering amplitudes in QCD at NNLO to higher orders in the dimensional regulator*, *JHEP* **12** (2019) 177, [1910.06684].
- [9] F. Caola, A. Chakraborty, G. Gambuti, A. von Manteuffel and L. Tancredi, *Three-loop helicity amplitudes for four-quark scattering in massless QCD*, *JHEP* **10** (2021) 206, [2108.00055].
- [10] F. Caola, A. Chakraborty, G. Gambuti, A. von Manteuffel and L. Tancredi, *Three-loop helicity amplitudes for quark-gluon scattering in QCD*, *JHEP* **12** (2022) 082, [2207.03503].
- [11] F. Caola, A. Chakraborty, G. Gambuti, A. von Manteuffel and L. Tancredi, *Three-Loop Gluon Scattering in QCD and the Gluon Regge Trajectory*, *Phys. Rev. Lett.* **128** (2022) 212001, [2112.11097].
- [12] A. V. Kotikov, *Differential Equations and Feynman Integrals*, in *Antidifferentiation and the Calculation of Feynman Amplitudes*, 2, 2021. **2102.07424**. DOI.
- [13] T. Gehrmann and E. Remiddi, *Differential equations for two-loop four-point functions*, *Nucl. Phys. B* **580** (2000) 485–518, [hep-ph/9912329].
- [14] J. M. Henn, *Multiloop integrals in dimensional regularization made simple*, *Phys. Rev. Lett.* **110** (2013) 251601, [1304.1806].
- [15] K. G. Chetyrkin and F. V. Tkachov, *Integration by parts: The algorithm to calculate β -functions in 4 loops*, *Nucl. Phys. B* **192** (1981) 159–204.
- [16] S. Laporta, *High-precision calculation of multiloop Feynman integrals by difference equations*, *Int. J. Mod. Phys. A* **15** (2000) 5087–5159, [hep-ph/0102033].
- [17] Z. Bern, L. J. Dixon and A. Ghinculov, *Two loop correction to Bhabha scattering*, *Phys. Rev. D* **63** (2001) 053007, [hep-ph/0010075].
- [18] Z. Bern, A. De Freitas, L. J. Dixon, A. Ghinculov and

- H. L. Wong, *QCD and QED corrections to light by light scattering*, *JHEP* **11** (2001) 031, [[hep-ph/0109079](#)].
- [19] C. M. Carloni Calame, M. Chiesa, S. M. Hasan, G. Montagna, O. Nicrosini and F. Piccinini, *Towards muon-electron scattering at NNLO*, *JHEP* **11** (2020) 028, [[2007.01586](#)].
- [20] P. Banerjee, T. Engel, N. Schalch, A. Signer and Y. Ulrich, *Bhabha scattering at NNLO with next-to-soft stabilisation*, *Phys. Lett. B* **820** (2021) 136547, [[2106.07469](#)].
- [21] R. Bonciani et al., *Two-Loop Four-Fermion Scattering Amplitude in QED*, *Phys. Rev. Lett.* **128** (2022) 022002, [[2106.13179](#)].
- [22] E. Budassi, C. M. Carloni Calame, M. Chiesa, C. L. Del Pio, S. M. Hasan, G. Montagna, O. Nicrosini and F. Piccinini, *NNLO virtual and real leptonic corrections to muon-electron scattering*, *JHEP* **11** (2021) 098, [[2109.14606](#)].
- [23] A. Broggio et al., *Muon-electron scattering at NNLO*, *JHEP* **01** (2023) 112, [[2212.06481](#)].
- [24] S. Kollatzsch and Y. Ulrich, *Lepton pair production at NNLO in QED with EW effects*, *SciPost Phys.* **15** (2023) 104, [[2210.17172](#)].
- [25] S. Badger, J. Kryś, R. Moodie and S. Zoia, *Lepton-pair scattering with an off-shell and an on-shell photon at two loops in massless QED*, *JHEP* **11** (2023) 041, [[2307.03098](#)].
- [26] M. Delto, C. Duhr, L. Tancredi and Y. J. Zhu, *Two-Loop QED Corrections to the Scattering of Four Massive Leptons*, *Phys. Rev. Lett.* **132** (2024) 231904, [[2311.06385](#)].
- [27] V. S. Fadin and R. N. Lee, *Two-loop radiative corrections to $e^+e^- \rightarrow \gamma\gamma^*$ cross section*, *JHEP* **11** (2023) 148, [[2308.09479](#)].
- [28] P. Banerjee et al., *Theory for muon-electron scattering @ 10 ppm: A report of the MUonE theory initiative*, *Eur. Phys. J. C* **80** (2020) 591, [[2004.13663](#)].
- [29] R. Aliberti et al., *Radiative corrections and Monte Carlo tools for low-energy hadronic cross sections in e^+e^- collisions*, [2410.22882](#).
- [30] J. L. Bourjaily et al., *Functions Beyond Multiple Polylogarithms for Precision Collider Physics*, in *Snowmass 2021*, 3, 2022. [2203.07088](#).
- [31] L. Chen, *A prescription for projectors to compute helicity amplitudes in D dimensions*, *Eur. Phys. J. C* **81** (2021) 417, [[1904.00705](#)].
- [32] T. Peraro and L. Tancredi, *Physical projectors for multi-leg helicity amplitudes*, *JHEP* **07** (2019) 114, [[1906.03298](#)].
- [33] T. Peraro and L. Tancredi, *Tensor decomposition for bosonic and fermionic scattering amplitudes*, *Phys. Rev. D* **103** (2021) 054042, [[2012.00820](#)].
- [34] G. 't Hooft and M. J. G. Veltman, *Regularization and Renormalization of Gauge Fields*, *Nucl. Phys. B* **44** (1972) 189–213.
- [35] C. Gnendiger et al., *To d , or not to d : recent developments and comparisons of regularization schemes*, *Eur. Phys. J. C* **77** (2017) 471, [[1705.01827](#)].
- [36] G. Crisanti, T. Dave, S. Smith, M. Mandal, P. Mastrolia, J. Ronca and W. J. Torres Bobadilla, *In preparation*, .
- [37] J. Henn, B. Mistlberger, V. A. Smirnov and P. Wasser, *Constructing d -log integrands and computing master integrals for three-loop four-particle scattering*, *JHEP* **04** (2020) 167, [[2002.09492](#)].
- [38] J. M. Henn and W. J. T. Bobadilla, *Maximal transcendental weight contribution of scattering amplitudes*, *JHEP* **03** (2022) 174, [[2112.08900](#)].
- [39] A. B. Goncharov, *Multiple polylogarithms, cyclotomy and modular complexes*, *Math. Res. Lett.* **5** (1998) 497–516, [[1105.2076](#)].
- [40] J. Hoff, *The Mathematica package TopoID and its application to the Higgs boson production cross section*, *J. Phys. Conf. Ser.* **762** (2016) 012061, [[1607.04465](#)].
- [41] M. Gerlach, F. Herren and M. Lang, *tapir: A tool for topologies, amplitudes, partial fraction decomposition and input for reductions*, *Computer Physics Communications* **282** (Jan., 2023) 108544.
- [42] V. Shtabovenko, *FeynCalc goes multiloop*, *J. Phys. Conf. Ser.* **2438** (2023) 012140, [[2112.14132](#)].
- [43] P. Maierhöfer, J. Usovitsch and P. Uwer, *Kira—a feynman integral reduction program*, *Computer Physics Communications* **230** (Sept., 2018) 99–112.
- [44] T. Hahn, *Generating Feynman diagrams and amplitudes with FeynArts 3*, *Comput. Phys. Commun.* **140** (2001) 418–431, [[hep-ph/0012260](#)].
- [45] R. N. Lee, *Presenting litered: a tool for the loop integrals reduction*, 2012.
- [46] T. Peraro, *Finiteflow: multivariate functional reconstruction using finite fields and dataflow graphs*, *Journal of High Energy Physics* **2019** (July, 2019) .
- [47] A. von Manteuffel and R. M. Schabinger, *A novel approach to integration by parts reduction*, *Phys. Lett. B* **744** (2015) 101–104, [[1406.4513](#)].
- [48] T. Peraro, *Scattering amplitudes over finite fields and multivariate functional reconstruction*, *JHEP* **12** (2016) 030, [[1608.01902](#)].
- [49] X. Liu, Y.-Q. Ma and C.-Y. Wang, *A Systematic and Efficient Method to Compute Multi-loop Master Integrals*, *Phys. Lett. B* **779** (2018) 353–357, [[1711.09572](#)].
- [50] X. Liu and Y.-Q. Ma, *Amflow: A mathematica package for feynman integrals computation via auxiliary mass flow*, *Computer Physics Communications* **283** (Feb., 2023) 108565.
- [51] C. Duhr and F. Dulat, *Polylogtools — polylogs for the masses*, *Journal of High Energy Physics* **2019** (Aug., 2019) .
- [52] T. Becher, A. Broggio and A. Ferroglia, *Introduction to Soft-Collinear Effective Theory*. Springer International Publishing, 2015. 10.1007/978-3-319-14848-9.
- [53] L. J. Dixon, *Calculating scattering amplitudes efficiently*, in *Theoretical Advanced Study Institute in Elementary Particle Physics (TASI 95): QCD and Beyond*, pp. 539–584, 1, 1996. [hep-ph/9601359](#).
- [54] M. K. Mandal, P. Mastrolia, J. Ronca and W. J. Bobadilla Torres, *Two-loop scattering amplitude for heavy-quark pair production through light-quark annihilation in QCD*, *JHEP* **09** (2022) 129, [[2204.03466](#)].
- [55] P. Bärnreuther, M. Czakon and P. Fiedler, *Virtual amplitudes and threshold behaviour of hadronic top-quark pair-production cross sections*, *JHEP* **02** (2014) 078, [[1312.6279](#)].
- [56] V. Ahrens, M. Neubert and L. Vernazza, *Structure of Infrared Singularities of Gauge-Theory Amplitudes at Three and Four Loops*, *JHEP* **09** (2012) 138, [[1208.4847](#)].

- [57] T. Becher and M. Neubert, *Infrared singularities of QCD amplitudes with massive partons*, *Phys. Rev. D* **79** (2009) 125004, [0904.1021].
- [58] N. Kidonakis, *Two-loop soft anomalous dimensions with massive and massless quarks*, in *Meeting of the Division of Particles and Fields of the American Physical Society (DPF 2009)*, 10, 2009. 0910.0473.